UNIVERSIDADE FEDERAL DE PERNAMBUCO
CENTRO DE TECNOLOGIA E GEOCIÊNCIAS
DEPARTAMENTO DE ENGENHARIA DE PRODUÇÃO
PROGRAMA DE PÓS-GRADUAÇÃO EM ENGENHARIA DE PRODUÇÃO

LAVÍNIA MARIA MENDES ARAÚJO

PROGNOSTICS AND HEALTH MANAGEMENT VIA QUANTUM MACHINE LEARNING IN THE OIL & GAS INDUSTRY

Recife
2023

LAVÍNIA MARIA MENDES ARAÚJO

PROGNOSTICS AND HEALTH MANAGEMENT VIA QUANTUM MACHINE LEARNING IN THE OIL & GAS INDUSTRY

Master thesis presented to Programa de Pós Graduação em Engenharia de Produção of Universidade Federal de Pernambuco as part of the requirementsfor the master's degree attainment.

Concentration area: Operations Research.

Advisor: Profª. Drª. Isis Didier Lins.

Recife

2023

A663p Araújo, Lavínia Maria Mendes.
Prognostics and health management via quantum machine learning in the oil & gas industry / Lavínia Maria Mendes Araújo. 2023.
78 f: il.

Orientadora: Profa. Dra. Isis Didier Lins.
Dissertação (Mestrado) – Universidade Federal de Pernambuco. CTG. Programa de Pós-Graduação em Engenharia de Produção, Recife, 2023.
Inclui referências.
Textos em inglês.

1. Engenharia de produção. 2. Aprendizagem de máquinas quântica. 3. Gerenciamento de prognóstico e saúde. 4. Diagnóstico de falhas. 5. Indústria de petróleo e gás. 6. Pesquisa e desenvolvimento. I. Lins, Isis Didier (Orientadora). II. Título.

UFPE

658.5 CDD (22. ed.) BCTG / 2023 - 68

LAVÍNIA MARIA MENDES ARAÚJO

PROGNOSTICS AND HEALTH MANAGEMENT VIA QUANTUM MACHINE LEARNING IN THE OIL & GAS INDUSTRY

Master thesis presented to Programa de Pós Graduação em Engenharia de Produção of Universidade Federal de Pernambuco as part of the requirementsfor the master's degree attainment. Concentration area: Operations Research.

Approved in: 15/02/2023.

EXAMINATION BOARD

_____

Profª. Drª. Isis Didier Lins (Advisor)
Universidade Federal de Pernambuco

_____

Prof. Dr. Márcio José das Chagas Moura (Internal Examiner)
Universidade Federal de Pernambuco

_____

Prof. Dr. Askery Canabarro (External Examiner)
Universidade Federal de Alagoas

To my mother Valquíria.

To my grandmother Zélia.

ACKNOWLEDGEMENTS

I thank my guardian angel for guiding and illuminating my path so far.

All my gratitude to my mother, Valquíria, for being my biggest support and an endless source of love. Also, to *ma belle* vovó Zélia for helping to shape me and being my great inspiration. To my brothers, Isac and Josué, for all the affection.

A huge thank you to my partner, Rafael, for all the patience, love, advice, and support in my moments of stress during the master's journey.

To my always friends, Lucas, Gabriela, Renata, Nathalia, Mylenna, Isabella, Thayna, and Arthur for the encouragement they bring me.

A special thanks to my advisor, Professor Isis Lins, for all her contributions to this study, academic opportunities, and teachings granted to me during this period.

To Professor Márcio Moura for his rich contributions not only to this master's thesis but to the courses and articles developed.

To Professor Askery Canabarro, especially for helping with quantum computing related questions.

To my master's friends, Júlia, Gabrielly, Fabiana, Fernanda, and Bruno, for their partnership throughout this journey.

To my colleagues from CEERMA, Plínio and July, for the friendly support and partnership on our projects. I also extend my appreciation to Professor Caio Souto Maior for his support throughout the studies we developed. Lastly, to Professor Paulo Estevão for his pertinent contributions to our formation through PRH 38.1.

To my grandfather Dedé for his investment in my education during elementary school. Furthermore, I am grateful for the quality of public educational institutions that have shaped me as a professional and citizen: IFPB, UFPB, and now UFPE.

Acknowledgement to the Graduate Program in Production Engineering (PPGEP-UFPE) for the academic opportunities, and to the Coordenação de Aperfeiçoamento de Pessoal de Nível Superior (CAPES) for the financial support in the development of this research.

Acknowledgement to the financial support from the Human Resources Program of the National Agency of Petroleum, Natural Gas and Biofuels - PRH-ANP, supported by resources derived from investment from qualified petroleum companies in the P, D&I Clause of ANP Resolution No. 50/2015.

“Não era como um quadro sem moldura. Era como a moldura de inúmeros quadros. Como quadros de uma fita de cinema. Vidas de luta e de coragem.” (Jorge Amado, Capitães da Areia)

ABSTRACT

The field of Prognostics and Health Management (PHM) aims to predict the behavior of machines to make informed maintenance decisions. In the Oil and Gas industry, fault mode diagnosis, as a PHM activity, has been applied to rotating machinery such as compressors, centrifugal pumps, and submersible motors using traditional Machine Learning (ML) and Deep Learning techniques. With the emergence of a new and rapidly growing research field called Quantum Computing (QC), there is now potential for even more efficient and accurate predictions. The QC has contributed to different purposes and contexts, such as optimization, artificial intelligence, simulation, cybersecurity, pharmaceutics, and the energy sector. Despite the current limitations of hardware, QC has been explored to improve the speed and efficiency of ML models. This master thesis focuses on the application of Quantum Machine Learning (QML) to diagnose rolling bearings which are essential components in rotating machinery, based on vibration signals. We apply hybrid models involving the encoding and construction of parameterized quantum circuits connected to a classical neural network, the Multi-Layer Perceptron (MLP). The study uses the Variational Quantum Eigensolver framework along with rotation gates and different entanglement (two-qubits) gates (CNOT, CZ and *i*SWAP), and explores the impact of varying the number of layers (1, 5 and 10) in the quantum circuit. We use two databases of different complexity levels not previously explored with QML, namely Case Western Reserve University (CWRU) and Jiangnan University (JNU), with 10 and 12 failure modes, respectively. For CWRU and JNU, all QML models presented higher accuracy than the classical MLP. These results suggest that, despite the current limitations of quantum environments, QML models are promising tools to be further investigated in PHM activities in the Oil and Gas industry.

Keywords: quantum machine learning; prognostic and health management; fault diagnosis; oil and gas industry; research and development.

RESUMO

A área de Prognóstico e Gerenciamento de Saúde – *Prognostic and Health Management* (PHM) tem como objetivo prever o comportamento das máquinas para tomar decisões relacionadas a manutenção. Na indústria de Óleo e Gás, o diagnóstico de modo de falha, como uma atividade de PHM, tem sido aplicado em máquinas rotativas, como compressores, bombas centrífugas e motores submersos, usando técnicas tradicionais de Aprendizagem de Máquina (*Machine Learning* - ML) e Aprendizagem Profunda. Com o surgimento de um novo e crescente campo de pesquisa chamado Computação Quântica (*Quantum Computing* - QC), existe o potencial para previsões ainda mais eficientes e precisas. A QC tem contribuído para diferentes propósitos e contextos, como otimização, inteligência artificial, simulação, cibersegurança, indústria farmacêutica e setor energético. Apesar das limitações atuais de hardware, a QC tem sido explorada como uma maneira de melhorar a velocidade e eficiência dos modelos de ML. Este estudo se concentra na aplicação do Aprendizado de Máquina Quântica (*Quantum Machine Learning* - QML) para diagnosticar rolamentos, que são componentes essenciais em máquinas rotativas, com base em sinais de vibração. Aplicamos modelos híbridos que envolvem a codificação e construção de circuitos quânticos parametrizados conectados a uma rede neural clássica, a Perceptron de Camadas Múltiplas (*Multilayer Perceptron* - MLP). O estudo usa o *framework* Variational Quantum Eigensolver juntamente com portões de rotação e diferentes portões de emaranhamento (*two*-qubit *gates*), e explora o impacto de variar o número de camadas (1, 5 e 10) no circuito quântico. Usamos duas bases de dados de diferentes níveis de complexidade que não foram previamente exploradas com QML, a saber, Case Western Reserve University (CWRU) e Jiangnan University (JNU), com 10 e 12 modos de falha, respectivamente. Para a CWRU e para a JNU, todos os modelos QML apresentaram maior precisão do que o MLP clássico. Estes resultados sugerem que, apesar das limitações atuais dos ambientes quânticos, os modelos de QML são ferramentas promissoras para serem investigadas nas atividades de PHM na indústria de Óleo e Gás à medida que a QC avança.

Palavras-chave: aprendizagem de máquinas quântica; gerenciamento de prognóstico e saúde; diagnóstico de falhas; indústria de petróleo e gás; pesquisa e desenvolvimento.

LIST OF FIGURES

LIST OF TABLES

CONTENTS

1 INTRODUCTION

1.1 INITIAL REMARKS

An important contributor in power production worldwide is the Oil and Gas (O&G) industry (PERRONS, 2014). However, facing the climate changes, Tamala *et al*. (2022) present the reduction of the world's CO_2 emission as a major challenge to be faced by this sector. Ritchi *et al*. (2022) indicate that, in Brazil, the CO_2 emission in 2020 by oil and gas fuels resulted in 305.51 and 60.33 million tonnes, respectively. Those are the largest emissions in the country, respectively, 65.37% and 12.91% of the total (Figure 1). Besides the effectiviness and viability of the fossil fuels energy sources, the renewable energy fountains are emerging by the advance of new technologies with the advantage of less greenhouse gases emissions.

Figure 1 – CO_2 emissions by fuel type in Brazil.

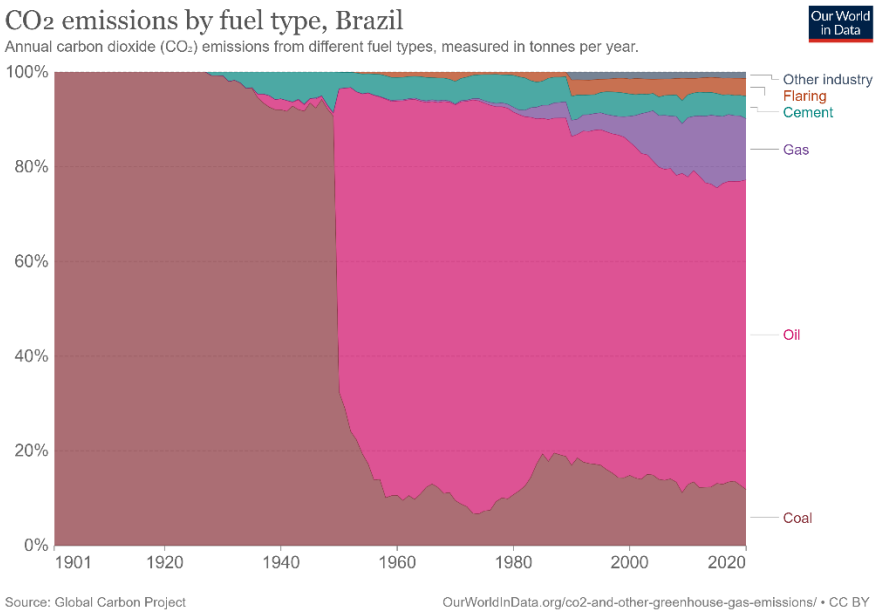

Source: Ritchie *et al*. (2020).

In addition, Perrons (2014) states that the O&G industry has changed in two critical aspects while global demand for these resources persists. The first is the large volume of "easy oil" that has already been consumed. As a result of this shift, upstream oil and gas businesses will need to invest in more complex technologies (ARAÚJO *et al*., 2022a) as exploring locations that are more challenging to access. Second, catastrophic disasters, such as the Deepwater Horizon oil spill (BEYER *et al*., 2016), have shifted O&G companies' expectations and standards regarding environmental management, safety, and human welfare

(CHANDRASEGARAN; GHAZILLA; RICH, 2020). O&G facilities, such as drilling ships, FPSOs (Floating, Production, Storage, and Offloading), and refineries, work to increase the efficiency of their operations and maintenance procedures to decrease downtimes and avoid failures (BARRAZA *et al*., 2022).

Based on the problems mentioned above and since O&G industry is a capital-intensive sector of the economy, strict availability standards are needed for its operations and innovative activities, from the creation and development to the operation of new technologies and equipment (BARRAZA *et al*., 2022). For example, in the mid-1970s, NASA developed the Technology Readiness Levels (TRL) approach that estimates the technologies' maturity during acquisition and availability for use in the field (OLECHOWSKI; EPPINGER; JOGLEKAR, 2015). Besides the aerospace sector, TRLs method was disseminated by ISO 16290:2013 to the other industries, including the O&G, alternative energy and defense industries (OLECHOWSKI; EPPINGER; JOGLEKAR, 2015; TOMASCHEK *et al*., 2016; YE *et al*., 2017).

The Bureau of Safety and Environmental Enforcement (BSEE) has adapted TRL for the O&G context. The steps are presented in Table 1. Each TRL represents general activities related to (1) technology research and development, (2) technology advancement, development, and demonstration, (3) technology deployment in operational environments, and (4) technology deployment in real environment.

Table 1 – BSEE TRLs

TRL	**Title**
	Technology Research and Development
1	Basic principles observed or reported
2	Technology concept and speculative application formulated
3	Technology proof of concept demonstrated
	Technology Advancement, Development, and Demonstration
4	Technology prototype demonstrated in laboratory environment or model scenario
5	Technology prototype tested in relevant environments
6	Full-scale prototype demonstrated in relevant environments
	Technology Implementation in Operational Environments
7	Integrated technology tested on a large scale
8	Final integrated system tested in a real or relevant environment
	Technology Deployment in Real Environment

9	A final integrated system deployed in a real environment

Source: Adapted from Panetta and Potter (2016, p. 5).

As equipment development progresses in TRLs, an approach goes along with it, which is Prognostics and Health Management (PHM). PHM uses past and present information about equipment to assess its health, diagnose, predict and manage failures (JAVED; GOURIVEAU; ZERHOUNI, 2017). In Table 1, the PHM execution can be primarily inserted from TRL 6 onwards, where testing and monitoring are performed to diagnose the condition and predict, for example, the Remaining Useful Life (RUL) of equipment. Although the PHM is usually applied form TRL 6 and has its real-time execution in TRL 9, the planning should be considered already in TRL 1, to define the parameters to be analyzed, as well as the tests and operations to be carried out to collect the data (JAVED; GOURIVEAU; ZERHOUNI, 2017; ROYCHOUDHURY *et al*., 2013), as shown in Figure 2.

Figure 2 – Concept of TRLs adopted to represent prognostics maturity

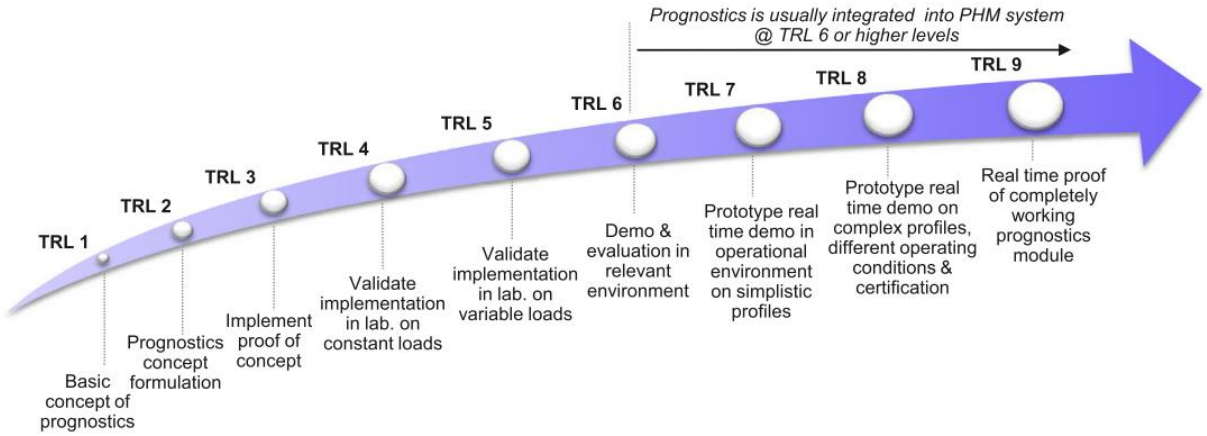

Source: Javed; Gouriveau; Zerhouni (2017, p. 217).

Besides contributing to the context of equipment development, PHM tasks are also applied in the context of maintenance of in-use equipment. Mainly in the Condition Based Maintenance (CBM), which several businesses have implemented (e.g., automotive, aerospace, and military sectors) (QUATRINI *et al*., 2020). In this case, the monitoring and analysis of equipment conditions are constantly performed (ZONTA *et al*., 2020). The maintenance programs are proactive so that decisions are taken when there is a tendency to fail. Equipment degradation diagnoses and prediction are performed so that critical system failures and system shutdowns are avoided (BARRAZA *et al*., 2022; KUMAR; SHANKAR; THAKUR, 2018).

The three major stages of CBM are data capture, data processing, and maintenance decision-making. Such steps must be performed for diagnosis or prognosis (ZONTA *et al*., 2020).

Diagnostics in the PHM can be characterized as detecting present-day failures and providing information about potential outcomes. On the other hand, prognostics is the forecasting of future failures, or what is most likely to occur (BARRAZA *et al*., 2022; CORREA-JULLIAN *et al*., 2022; JAVED; GOURIVEAU; ZERHOUNI, 2017; LINS *et al*., 2015; SONG; WANG; CHEN, 2018).

Traditional intelligent diagnosis methods include feature extraction using signal processing methods and fault classification by adopting Machine Learning (ML) and Deep Learning (DL) approaches (LUCAS *et al*., 2022; WANG *et al*., 2017; ZHAO *et al*., 2020). For example, Lucas *et al*. (2022) used Variational Autoencoder to diagnose failure modes of rotating machinery components. For the same category of equipment Zhao *et al*. (2020) present a study that serves as a benchmark with different DL models applied to different databases available in the literature. Among the techniques, there are Multi-layer Perceptron (MLP), Autoencoder (AE), Convolutional Neural Network (CNN), Recurrent Neural Network (RNN) and Deep Belief Network (DBN).

PHM studies have been designed for the O&G sector to ensure safe and dependable output. Submersible motors were studied in Zhang and Yang (2022) paper; they are crucial elements of the offshore platform's producing machinery. For the extraction of oil and gas, the supply of natural gas for electricity, and other social and economic benefits, submersible motor operation reliability is essential. The authors suggested a motor fault monitoring method based on multi-signal fusion to perform the PHM of this equipment. As distinctive signals, current and vibration have been chosen. Orrù *et al*. (2020) applied MLP and Support Vector Machine (SVM) for the failure prediction of a centrifugal pump in an Italian refinery. The predictive model attributes include flow rate, bearing vibration, axial displacement, and motor winding temperature. A petroleum refinery's rolling bearings are subjected to vibration monitoring by Orhan, Aktürk, and Çelik (2006) to use the analysis as a preventive maintenance method. To identify faults early on, they employ spectral analysis. Finally, Moradi *et al*. (2022) performed analyses on Vapor Recovery Unit compressors using Bayesian DL models.

Recently, important research interest has emerged based on the tremendous potential of parallelism offered by Quantum Computing (QC) and related quantum technologies (NAWAZ *et al*., 2019). Quantum algorithms aim to find ways to speed up the solution of computational problems by using a quantum computer (HARROW; MONTANARO, 2017). A quantum machine characterizes and computes the quantum properties of an atom in a molecule, which

is computationally and exceedingly challenging even for a supercomputer to handle. This significantly impacts drug research, healthcare, and big data processing (KAVITHA; KAULGUD, 2022).

Machine learning and QC are both likely to play a role in how society deals with information in the future, so it is logical to wonder how they could be merged (KAVITHA; KAULGUD, 2022; SIERRA-SOSA; TELAHUN; ELMAGHRABY, 2020), mainly because QC's prospects are increasing faster in hardware performance. For example, it is possible to evaluate several states simultaneously because quantum computations are based on the idea that subatomic particles can exist simultaneously in several states. It may lead to significant speedups (KHAN; ROBLES-KELLY, 2020) conferring, then, a possibility to improve the classic ML (BIAMONTE *et al*., 2017), since for many scenarios, as the amount of data grows, aligned with the complexity of the information, the training process becomes slower (ZHAO *et al*., 2020). It is one of the many applications that could profit from quantum devices (PERDOMO-ORTIZ *et al*., 2018). In this context, some machine learning models with quantum properties have appeared recently in the field of tools for the classification process (BIAMONTE *et al*., 2017; CORREA-JULLIAN *et al*., 2022; GARCÍA; CRUZ-BENITO; GARCÍA-PEÑALVO, 2022; SILVA; DROGUETT, 2022). It is one of the many applications that could profit from quantum devices (PERDOMO-ORTIZ *et al*., 2018).

ML applications incorporating quantum techniques are known as Quantum Machine Learning (QML). QML models are based on QC techniques to develop new algorithms and improve existing ones (GARCÍA; CRUZ-BENITO; GARCÍA-PEÑALVO, 2022; SILVA; DROGUETT, 2022). Indeed, QC and ML are the two key areas that play a crucial role in engineering science as technology is developing quickly (ARAÚJO *et al*., 2022b, 2022c).

This study will explore QML models to diagnose failure modes of different components and equipment with two bearing dataset available in the literature (CWRU, 2020; JNU, 2019) that are amenable to use in the O&G industry. Although QC is promising, there are still limitations. For example, the number of quantum units, i.e., qubits is still limited in simulators and quantum machines. Note that a qubit is the smallest unit of information in a quantum computer and can be either 0 or 1 or a superposition of these two (WANG; LIU, 2022).

The ability to be in superposition is one of the qualities that distinguish a qubit from a conventional bit. One way to conceptualize a quantum state in superposition is as a linear combination of other unique quantum states. The core idea is that a search algorithm can tunnel through energetic barriers to escape local minima because quantum superposition and tunneling

enable direct transitions between states even when there is a high energy barrier between them (YARKONI *et al*., 2021).

Therefore, this work aims, above all, to investigate the applicability of these techniques in the evaluation of vibration signals and compare them with classical ML models. The approaches will be tested on rotating machine components subjected to vibration as a stressor, common in O&G industry systems (KHALAF; SEIBI, 2011; ORRÙ *et al*., 2020). These machines are an essential industrial component of contemporary. For instance, motors have provided more than 50% of the mechanical energy supply for industrial applications in the United States (SONG; WANG; CHEN, 2018). The performance and operational efficiency of rotating machines are significantly impacted by bearings, which account for about 40% of electrical motor failure incidents machinery (SONG; WANG; CHEN, 2018). Vibrational analysis has become the industry standard for assessing the condition of roller bearings and other rotating machinery (ZHAO *et al*., 2019). Equipment and components can be better shielded from breaking if bearing issues can be recognized quickly and precisely (SONG; WANG; CHEN, 2018; ZHAO *et al*., 2020).

Moreover, besides rotation gates, we apply entanglement gates (CNOT, CZ, and *i*SWAP) and more layers in the Parameterized Quantum Circuit (PQC) to observe the effect of such model variations. Entanglement is the phenomenon where two particles can be connected independent of the distance (KAVITHA; KAULGUD, 2022). The hypothesis is that the time and computing power needed will be reduced since one qubit can provide information about the other unit to which it is related (KHAN; ROBLES-KELLY, 2020).

Note that the current investigation employs a quantum simulator sourced from the TensorFlow Quantum library to execute the QML models. Consequently, there are no direct assessments made on quantum hardware. Also, the potential influence of quantum noise is not factored into the analysis.

In addition, our study will be applied to two complex databases available in the literature that have not yet been explored in the context of QML. Those are bearing datasets: (1) Case Western Reserve University (CWRU, 2020) and (2) Jiangnan University (JNU, 2019). The results obtained from the application of these models aim to indicate the QML's usability and importance in supporting decision-making related to maintenance.

1.2 RATIONALE AND CONTRIBUTION

Companies have been investing in Research and Development (R&D) as it represents a key factor for economic and competitive growth (ARAÚJO *et al*., 2021). Mavrotas and Makryvelios (2021) add that high-impact projects in this area are urgent and crucial for various organizations. The creation of new technologies or equipment poses many technical obstacles, including enhancements to existing operational methods and equipment and disruptive developments. The reliability and qualification of the equipment are crucial considerations in both circumstances during the design process. The development process should be based on reliability, PHM and allow for uncertainty (MAIOR *et al*., 2022; SHAFIEE; ELUSAKIN; ENJEMA, 2020; SHARMA; CHANDA, 2017). Throughout the development of the technology, studies have evaluated its reliability (JAVED; GOURIVEAU; ZERHOUNI, 2017; MAIOR *et al*., 2022; YE *et al*., 2017). Maior *et al*. (2022) indicate that estimating reliability is critical for ensuring predictability in equipment and technologies installed in oil wells.

PHM systems are decisive to minimizing downtime and maintenance expenses and ensuring the safe and proper operation of real-world designed systems (ROYCHOUDHURY *et al*., 2013). The PHM community has utilized deep learning for almost ten years to handle issues like the identification of rotating machinery's health states, the prediction of remaining useful life, or Bayesian analysis within complex and networked systems (ORRÙ *et al*., 2020; ROYCHOUDHURY *et al*., 2013; SAIMURUGAN *et al*., 2011; SONG; WANG; CHEN, 2018; ZHAO *et al*., 2020).

Nevertheless, the quantum supremacy experiment and the first computers becoming accessible to the general public through cloud services have sparked interest in the field of quantum computing over the past three years in the general media and research community (HARROW; MONTANARO, 2017). This interest stems from the desire to find ways to optimize and accelerate current algorithms, modify them, or create new ones that take advantage of quantum mechanics (GARCÍA; CRUZ-BENITO; GARCÍA-PEÑALVO, 2022; RIEFFEL; POLAK, 2011; SILVA; DROGUETT, 2022).

Thus, this dissertation is justified because, to the best of our understanding, this is the first work to present the application of a QML model which classifies more than three health states of equipment component that can be used in the context of O&G industry. Moreover, besides rotation gates, we apply entanglement gates (CNOT, CZ and *i*SWAP) which correlates two quantum particles. Also, we aggregate more circuit gates architectures layers in the Parameterized Quantum Circuit (PQC) to observe the effect of such quantum properties. The results obtained from the application of these models aim to indicate their usability and importance in supporting decision-making related to maintenance.

Finally, this research is justified and states its relevance in three aspects: (1) social, (2) environmental, and (3) economic. In the social aspect, equipment health management provides society with safer and more reliable services. Moreover, one can consider the reduction of occupational accidents. The support of automated PHM systems helps operators who are directly involved in the operation since it reduces work pressure. Nevertheless, we point out that such techniques support but by no means replace the human element of the process. At the environmental level, the early diagnosis of failure modes for technologies can prevent leaks and minimize the emission of greenhouse gases. In the economic sense this thesis can help companies to reduce costs in several aspects. For example, the cost of accidents involving people, systems, and the environment. Furthermore, more efficient maintenance policies contribute to the reduction of expenses when performing preventive stops. It also promotes the preparation of the team and the necessary materials according to the plans.

1.3 OBJECTIVES

1.3.1 General Objective

The general objective of this study is to investigate and adapt QML models to perform the PHM, through fault mode diagnosis, of equipment suitable for application in the O&G.

1.3.2 Specific objectives

Given the general objective of this research, some specific objectives are defined:

- To investigate QML models with different structures of PQCs;
- To investigate works that address quantum machine learning models applied to the context of O&G;
- To diagnose failure modes of different equipment through quantum machine learning models;
- To test various PQCs with rotation and two-qubit gates combined with different amounts of layers;
- To perform a comparison between the models in terms of accuracy to test the technical feasibility of the models, i.e. to carry out proof of concept of this methodology.

1.4 DISSERTATION STRUCTURE

Besides the introduction section, the remainder of this work is structured as follows:

- Chapter 2 presents the theoretical framework that discusses PHM, Vibration Signals, Quantum Computing, and QML. Nevertheless, a literature review outlines what already exists in publications, as well as current gaps;
- Chapter 3 presents the methodological aspects of the study. Thus, a framework is outlined for the QML model. Furthermore, the databases used for the analyses are detailed;
- Chapter 4 presents the results concerning the QML models;
- Chapter 5 presents the conclusive aspects, the work's contributions, and suggestions for future research.

2 THEORETICAL BACKGROUND AND PRELIMINARY LITERATURE REVIEW

This section is divided into two main parts. The first is the theoretical background supporting the research. The second part is related to the literature review to identify the studies developed regarding the theme and the associated potential for innovation.

2.1 BEARINGS AND VIBRATION SIGNALS

Rolling bearings are essential parts of rotating machines, and investigation into their fault diagnosis is extensive (MAIOR; MOURA; LINS, 2019). Such studies are important since the failures result in equipment damage, production losses, and staff injuries (ZHANG *et al*., 2021). The outer race, inner race, ball, and cage are often the primary components taken into account in the study of localized faults in rolling bearings (ISLAM; KIM, 2019).

Signals for monitoring information (data) can be generically categorized into vibration and auditory, temperature, and wear debris analysis categories. To simultaneously save maintenance costs and downtime, a technique called vibration analysis is utilized to monitor machine operating conditions and to diagnose deteriorations (MAIOR *et al*., 2022; ORHAN; AKTÜRK; ÇELIK, 2006).

Vibration signals have a distinct pattern in a fault state than in a healthy state, allowing failure diagnosis. In fact, the acceleration signals exhibit a variety of broadband impulse responses due to localized failures in the rolling bearing components. As seen in Figure 3, the outer and inner races, as well as the ball, each have their own rotational frequency and wave behavior, resulting in a composed and complicated signal.

Figure 3 - Local rolling element bearing failure signals.

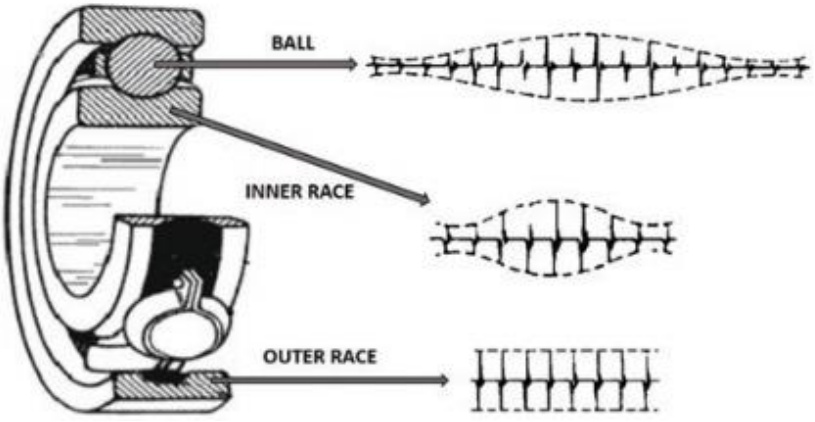

Source: Maior; Moura; Lins (2019, p. 611).

2.2 QUANTUM COMPUTING

Part of the content of this chapter was published and presented at the The Probabilistic Safety Assessment & Management (PSAM) conference (ARAÚJO *et al*., 2022b).

If the ability to simulate classical computers were the only feature of quantum computers, there would be little point in going to all the trouble of exploiting quantum effects. The advantage of quantum computing is that much more powerful functions may be computed using qubits and quantum gates.

The performance mechanisms in resolving important industrial problems are highlighted by the distinctions between classical computing and QC. The QC mechanics use fundamental quantum properties like superposition, entanglement, and the measurement paradox to find the best answers to challenging issues (OSABA *et al*., 2021; PRAKASH, 2021).

The smallest unit of information in a Quantum Computer is the qubit. The qubit can be either 0 or 1 or a superposition of these two. In quantum physics, Dirac's notation, namely bra/ket, is used to represent a quantum state and their transformation. The ket is represented by $|\psi\rangle$ and it has a dual called bra $\langle\psi|$ (RIEFFEL; POLAK, 2011). Eq. (1) provides the qubit state representation (CHIANG *et al*., 2014; PRAKASH, 2021).

$$|\psi\rangle = \alpha|0\rangle + \beta|1\rangle \tag{1}$$

Where α and β are complex numbers that represent amplitudes, and they satisfy the relation $|\alpha|^2 + |\beta|^2 = 1$; thus, $|\alpha|^2$ and $|\beta|^2$ are the probabilities of a qubit collapsing to states "0" or "1", respectively, after a measurement. Eq. (1) can be rewritten as Eq. (2), in which the parameters θ, ϕ, and γ are real numbers. (GARCÍA; CRUZ-BENITO; GARCÍA-PEÑALVO, 2022; PRAKASH, 2021; YARKONI *et al*., 2021).

$$|\psi\rangle = e^{i\gamma}\left(\cos\frac{\theta}{2}|0\rangle + e^{i\phi}\sin\frac{\theta}{2}\Big|1\rangle\right) \tag{2}$$

The Bloch Sphere (Figure 4) is a geometric representation of the pure state space of a two-level quantum mechanical system. It is used in quantum mechanics and computation (SCHERER, 2019). In Figure 4, the angles θ and ϕ correspond to spherical coordinates that represent a point describing a single qubit state (PRAKASH, 2021). The $|\boldsymbol{\psi}\rangle$ can be defined as a Hilbert Space vector coming from the origin to the sphere's surface. This vector has a $\mathbb{R}^{\mathbf{3}}$

dimension with the following configuration: [sin(θ)cos(ϕ), sin(θ)sin(ϕ), cos(ϕ)] (SCHULD; PETRUCCIONE, 2018).

Figure 4 - Bloch Sphere which represents the qubit.

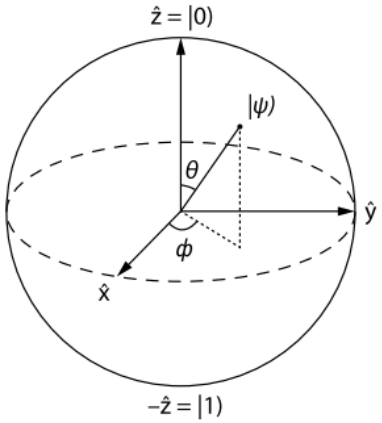

Source: Prakash (2021, p. 268).

Also, the Bloch sphere provides a visual representation of quantum states operations. Rotations on the sphere represent unitary transformations, while projections onto one of the poles depict measurements. The Bloch sphere's utility lies in its ability to show the impact of quantum gates, which form the foundation of quantum circuits. This makes it a valuable tool for creating and examining quantum algorithms and error correction techniques (SCHERER, 2019; SCHÖNBERGER, 2022). Finally, The Bloch sphere visually represents entangled states between two quantum systems. When two systems are entangled, their combined state cannot be described by a single point on the sphere but by a region of it (SIM; JOHNSON; ASPURU-GUZIK, 2019).

In Figure 5, we can see a representation of a quantum circuit. The circuit is a QC paradigm that is comparable to classical circuits, in which a computation is made up of a series of quantum gates, measurements, and qubit initializations to known values. The circuit is read from left to right. Following the horizontal lines Figure 5, |0⟩ represent the input qubits in state “0”. Next are logic gates, such as single-qubit blocks Hadamard (H), X and Z gates, and two-qubit gates as CNOT. In summary, the measurement operation at the end of the line translates the quantum result into a classical one (NIELSEN; CHUANG, 2010).

Figure 5 - A Quantum Circuit example.

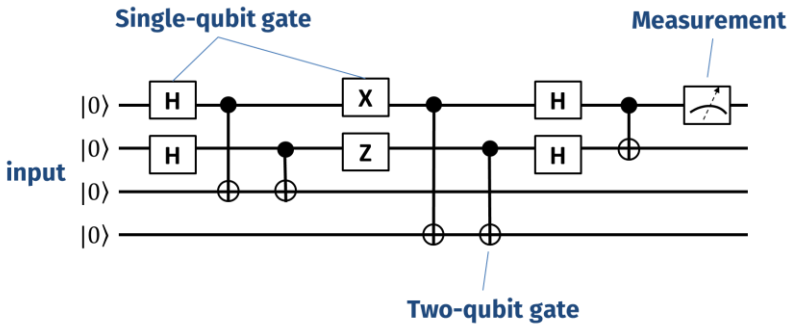

Source: Adapted from Nielsen and Chuang (2010).

The quantum operations are done according to a series of foundational operations called quantum logic gates. They are the building blocks behind all quantum algorithms (HARROW; MONTANARO, 2017; MONTANARO, 2016). The following sections present some of these gates, namely, superposition, controlled, and rotation gates.

2.2.1 The Hadamard Gate

A qubit can be forced into a superposition state using the Hadamard gate (Eq. 3). When applied over $|\Psi_0\rangle = |0\rangle$, its output is a qubit with an equal chance of going from a $|0\rangle$ or $|1\rangle$ state following a measurement (SHAREEF *et al.*, 2014; SILVA; DROGUETT, 2022).

$$H = \frac{1}{\sqrt{2}}\begin{bmatrix} 1 & 1 \\ 1 & -1 \end{bmatrix} \tag{3}$$

2.2.2 Controlled Gates

Entanglement is another important quantum mechanics property that is leveraged in quantum computing for constructing dependencies between qubits (CORREA-JULLIAN *et al.*, 2022). Among the entanglement gates, we can cite CNOT, CZ, and *i*SWAP as examples (RASMUSSEN; ZINNER, 2022).

Two inputs and two outputs make up the CNOT gate. If both qubits are in their absolute basal states, which are either $|0\rangle$ or $|1\rangle$, then the first qubit serves as the control qubit and the second acts as the controlled qubit. If the first qubit is $|0\rangle$, then the CNOT gate does not affect the system; if it is $|1\rangle$, the second qubit is inverted to the opposite state. That is if the second

qubit was |0⟩ it becomes |1⟩; if it was |1⟩, it becomes |0⟩ (CORREA-JULLIAN *et al*., 2022; SILVA; DROGUETT, 2022).

Target and controlled gates make up the CZ gate. If the controlled gate is 1, a Z gate was applied to the qubit on the target gate. A symmetric gate, the *i*SWAP switches two-qubit states and phases the amplitudes of |01⟩ and |10⟩ by i (NIELSEN; CHUANG, 2010; RASMUSSEN; ZINNER, 2022). Note that the kets cited above consist on the representation of two-qubits states. the Eqs. (4)-(6) present the matrices corresponding to these gates.

$$CNOT = \begin{bmatrix} 1 & 0 & 0 & 0 \\ 0 & 1 & 0 & 0 \\ 0 & 0 & 0 & 1 \\ 0 & 0 & 1 & 0 \end{bmatrix} \tag{4}$$

$$CZ = \begin{bmatrix} 1 & 0 & 0 & 0 \\ 0 & 1 & 0 & 0 \\ 0 & 0 & 1 & 0 \\ 0 & 0 & 0 & -1 \end{bmatrix} \tag{5}$$

$$iSWAP = \begin{bmatrix} 1 & 0 & 0 & 0 \\ 0 & 0 & i & 0 \\ 0 & i & 0 & 0 \\ 0 & 0 & 0 & 1 \end{bmatrix} \tag{6}$$

2.2.3 Rotation Gates

Since the Hadamard and CNOT gates work directly on qubits without requiring the definition of external parameters, they can be categorized as non-parametric gates. Rotation gates, on the other hand, can have their impact on a qubit fine-tuned externally, making them single qubit parametric gates (CHIANG *et al*., 2014; CORREA-JULLIAN *et al*., 2022; SILVA; DROGUETT, 2022).

The effect of the rotational gate operation can be simply understood thanks to the Bloch Sphere depiction. Each operation rotates the qubit by a specific number of radians determined by the external parameter, i.e., the parameterized rotation angle. This rotation is around the main axis. Eq. (7)-(9) provide the matrices for these gates (CHIANG *et al*., 2014; CORREA-JULLIAN *et al*., 2022; SILVA; DROGUETT, 2022).

$$R_x(\xi) = \begin{bmatrix} cos\frac{\xi}{2} & -i\ sin\frac{\xi}{2} \\ -i\ sin\frac{\xi}{2} & cos\frac{\xi}{2} \end{bmatrix} \tag{7}$$

$$R_y(\xi) = \begin{bmatrix} cos\frac{\xi}{2} & -sin\frac{\xi}{2} \\ sin\frac{\xi}{2} & cos\frac{\xi}{2} \end{bmatrix} \quad (8)$$

$$R_z(\xi) = \begin{bmatrix} e^{-i\frac{\xi}{2}} & 0 \\ 0 & e^{i\frac{\xi}{2}} \end{bmatrix} \quad (9)$$

2.3 LITERATURE REVIEW

2.3.1 Quantum Machine Learning applied to PHM in the O&G Industry

QC is frequently referred to as an interdisciplinary research frontier involving disciplines as diverse as computer science, physics, chemistry, and engineering. The excitement relies on the hypothesis that quantum information will eventually result in a new wave of technological advancements in information, computation, and communication (WANG; LIU, 2022).

QML is a new field of study that emerged by exploiting quantum systems to process classical data using ML techniques. Indeed, the field of computer science may undergo a radical change as a result of QML. Information processing could be accelerated far beyond current classical speeds. (KHAN; ROBLES-KELLY, 2020).

Despite novelty in the context of Reliability Engineering, QML has a growing interest in the academia, expanding its application in recent years. Figure 6, extracted from WoS, provides the number of articles using “Quantum Machine Learning” as a keyword. The first publication appeared in 2014 and, since then, this number has been increasing significantly. The year 2022 has the peak of publications, with 130 in total. The search was conducted until October 2022.

Figure 6 – “Quantum Machine Learning” publications in Web of Science.

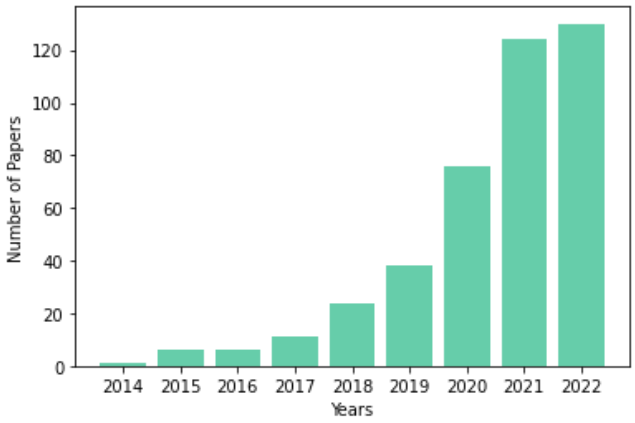

Source: The Author (2023).

The research community has shown interest in two strategies. The first, PQC, a quantum circuit made up of parametric gates is considered a trainable model, with the parameters being updated to minimize a specified objective function. PQC enables researchers to draw obvious similarities and parallels with classic neural networks The second strategy is related to quantum kernel techniques. They can be employed for prediction and tasks like clustering or dimensionality reduction (CORREA-JULLIAN *et al*., 2022; SILVA; DROGUETT, 2022).

Although these combined algorithms have theoretically demonstrated performance gains, their scalability is still in question because current Quantum Processing Units (QPUs) are unable to dependably execute the operations necessary to evaluate these methods on actual data. To examine the effects of incorporating quantum circuits as building blocks into new frameworks, a different strategy is to employ small, parameterized quantum circuits that can be easily operated on real hardware or even simulated in classical computers. In a sense, this method of tackling this new subject is comparable to what happened with DL models in the wake of ML models’ natural progression toward greater scalability around 2010 (GARCÍA; CRUZ-BENITO; GARCÍA-PEÑALVO, 2022; MONTANARO, 2016; SILVA; DROGUETT, 2022).

In a literature review, when searching by keywords in WoS, the combinations “Quantum Machine Learning” and “PHM” or “Fault Detection” only returned one article. In this case, the authors applied quantum kernel methods to wind turbine fault detection (CORREA-JULLIAN *et al*., 2022). Extending the search to Google Scholar, one more article is found exploring rotating machines (SILVA; DROGUETT, 2022). In QML models, the quantum part aims to provide trial states for the algorithm. The PQC, or ansatz circuit, generates these states

according to a set of control parameters that are managed by the classical part of the algorithm (RASMUSSEN; ZINNER, 2022).

PQC has been applied in the PHM context to categorize health states in rotating machinery with performance comparable to conventional ML methods (SILVA; DROGUETT, 2022). Nevertheless, in this case, only rotation gates were used.

It is necessary to observe the effect of operations such as superposition and entanglement to emphasize the quantum contribution of the model. Faced with the different ways of schematizing PQCs, there are algorithms that combine the two types of ports mentioned here (single-qubit and two-qubit), such as the Variational Quantum Eigensolver (VQE), that can combine the single-qubit and two-qubit, as well as the parameterized and non-parameterized gates (RASMUSSEN; ZINNER, 2022; TILLY *et al*., 2022). For example, Rasmussen and Zinner (RASMUSSEN; ZINNER, 2022) used VQE with both single (rotation gates) and two-qubit (CNOT, CZ, and *i*SWAP) gates with angles to be parameterized during training. Meanwhile, Sim *et al*. (SIM; JOHNSON; ASPURU-GUZIK, 2019) performed several combinations with different rotation gates, in x, y, and z, and entanglement gates (CNOT and CZ), forming 19 different circuit types for testing. Schuld and Petruccione (SCHULD; PETRUCCIONE, 2018) also add other circuit schematization possibilities, such as those based on the Quantum Approximate Optimization Algorithm (QAOA) architecture.

3 METHODOLOGY

This research is characterized by being of an applied nature due to its practical interest, that is, the results should be applied or used in solving problems that occur in reality (MARCONI; LAKATOS, 2002). Regarding its objectives, the research can be classified as exploratory. In this case, the procedures to be adopted are for investigations in which the object of research presents a lack of knowledge, i.e., in our focus, it is not widely explored in the literature (GIL, 2002; SCHOLTEN; BLOK; HAAR, 2015). This research has a Quantitative Approach because it considers that opinions and information can be translated into numbers and analyzed statistically (HABES *et al*., 2018). Finally, to address the objectives of this work concerning data, the Problem Modeling method will be adopted. It comprises the use of mathematical techniques to describe the operation of a system (GIL, 2002). Figure 7 contains the classification of the present study, according to approach, objectives, technical procedures, and nature.

Figure 7 – Research methodology classification

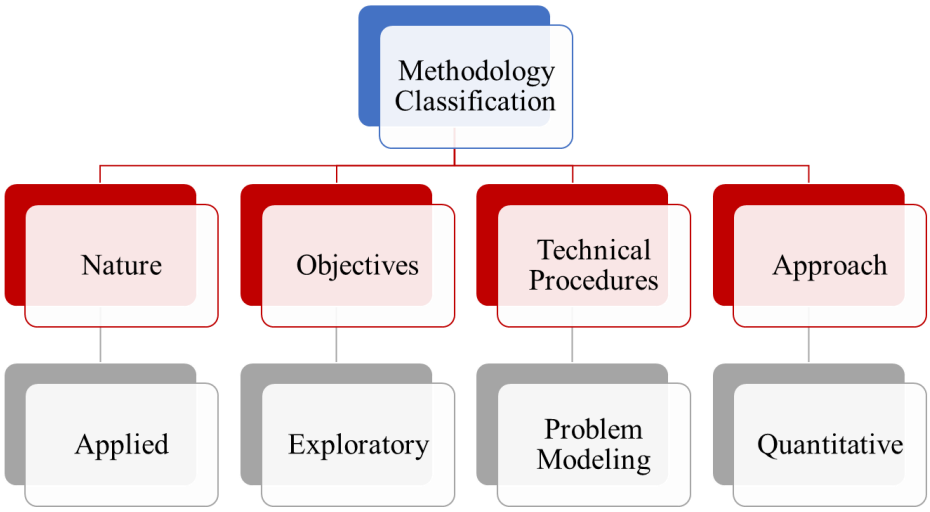

Source: The Author (2023)

3.1 DATASETS

3.1.1 CWRU dataset

The Bearing Data Center dataset from Case Western Reserve University (CWRU, 2020) is used in this study to assess the proposed methodology. This set includes signals from mechanical vibration series obtained from an induction electric motor with engine load starting from 0 to 3 HP. Data were obtained from two accelerometers mounted on top of the motor and

connected by magnetic bases, one of which was collected at the Drive End (DE), and the other was collected nearby the bearing Fan End (FE). The collections of the two accelerometers are precisely coordinated.

These faults, which can occur in the rearing Rolling Element (RE), the Inner Raceway (IR), and the Outer Raceway (OR), are intentionally introduced by an electro-discharge machine (EDM), additionally it having various fault widths and engine rotation rates (CWRU, 2020). Table 2 shows the different failure modes, the diameters used and the proportion of each class in the data set used. The vibration data are collected at a rate of 12k samples per second from accelerometers connected to the equipment at two points, at the upper and lower turbine of the device.

Table 2 – Description of failure modes of the CWRU.

Label	Mode Description	Proportion (%)
0	Health State: the normal bearing	18.24
1	Inner ring 1: 0.007 inch	9.04
2	Inner ring 2: 0.014 inch	9.12
3	Inner ring 3: 0.021 inch	9.12
4	Rolling Element 1: 0.007 inch	9.04
5	Rolling Element 2: 0.014 inch	9.04
6	Rolling Element 3: 0.021 inch	9.04
7	Outer ring 1: 0.007 inch	9.12
8	Outer ring 2: 0.014 inch	9.12
9	Outer ring 3: 0.021 inch	9.12

Source: Adapted from Lucas *et al*. (2022, p. 02).

3.1.2 JNU dataset

Jiangnan University's (JNU) (JNU, 2019; LI *et al*., 2013) bearing datasets are also freely available and are made up of three vibration datasets with three different rotating speeds (600, 800, and 1000 rpm), all of which were gathered at 50 kHz. One health condition and three failure modes are displayed in the JNU datasets (IR, OR, and RE). All states were measured at the same locations as the CWRU base. As a result, the total working conditions classes are twelve, as shown in Table 3 with the respective proportions for each state.

Table 3 – Description of failure modes of the JNU dataset.

Label	Mode Description	Proportion (%)
0	Inner ring 1: 600 rpm	5.55
1	Health State 1: 600 rpm	16.68
2	Outer ring 1: 600 rpm	5.55
3	Rolling Element 1: 600 rpm	5.55
4	Inner ring 2: 800 rpm	5.55
5	Health State 2: 800 rpm	16.68
6	Outer ring 2: 800 rpm	5.55
7	Rolling Element 2: 800 rpm	5.55
8	Inner ring 3: 1000 rpm	5.55
9	Health State 3: 800 rpm	16.68
10	Outer ring 3: 1000 rpm	5.55
11	Rolling Element 3: 1000 rpm	5.55

Source: Adapted from Lucas *et al*. (2022, p. 03).

3.2 VIBRATION SIGNAL PREPROCESSING

In this study the input data were used in two ways: (1) time domain; and (2) frequency domain (the Fast Fourier Transform—FFT is used). The time domain input uses the vibration signals without a preprocessing. We use the same data length adopted by Zhao *et al*. (2020): 1024 points. Indeed, the total number of samples (*L*) is obtained according to the Eq. (10). Where *C* is each signal length and floor refers to rounding towards minus infinity.

$$\mathrm{L} = \mathrm{floor}\left(\frac{\mathrm{C}}{1024}\right) \tag{10}$$

In the frequency domain input, we apply the FFT in each sample from the time domain, according to Eq. (11). The $y[k]$ is the FFT of the signal in a sequence-*L*.

$$y[k] = \sum_{l=0}^{L-1} e^{-2\pi j \frac{k_l}{L}} s[l] \tag{11}$$

After defining the input type, we use the Maximum–Minimum normalization to facilitate the ML or QML convergence. This normalization is calculated according to Eq. (12). Where s_i is the input signal, also, the minimun and maximum values of s_i are, respectively, s_i^{min} and s_i^{max}.

$$s_i^{normalize-1} = \frac{s_i - s_i^{min}}{s_i^{max} - s_i^{min}}, \qquad i = 1, 2, \dots, L \tag{12}$$

3.3 QUANTUM MACHINE LEARNING METHODOLOGY

The step-by-step framework application of QML models is presented in Figure 8. This is a framework based on different studies that use the PQC logic in QML models (KAVITHA; KAULGUD, 2022; SIERRA-SOSA; TELAHUN; ELMAGHRABY, 2020; SILVA; DROGUETT, 2022). However, in our case, several modifications were analyzed regarding the neural network used, PQC settings, and health status diagnosis. In fact, here we considered a more complex problem for which more than ten different labels are possible for the machinery diagnosis. Moreover, while in other studies only rotation gates were used (KONAR *et al.*, 2017; SILVA; DROGUETT, 2022), we aggregate two-qubit gates to observe quantum effects arising from entanglement. Of which we tested CNOT, CZ, and *i*SWAP. In terms of application, the Python® programming language was used along with the TensorFlow Quantum library (SIERRA-SOSA; TELAHUN; ELMAGHRABY, 2020).

Figure 8 – Hybrid Quantum Machine Learning scheme to perform PHM tasks.

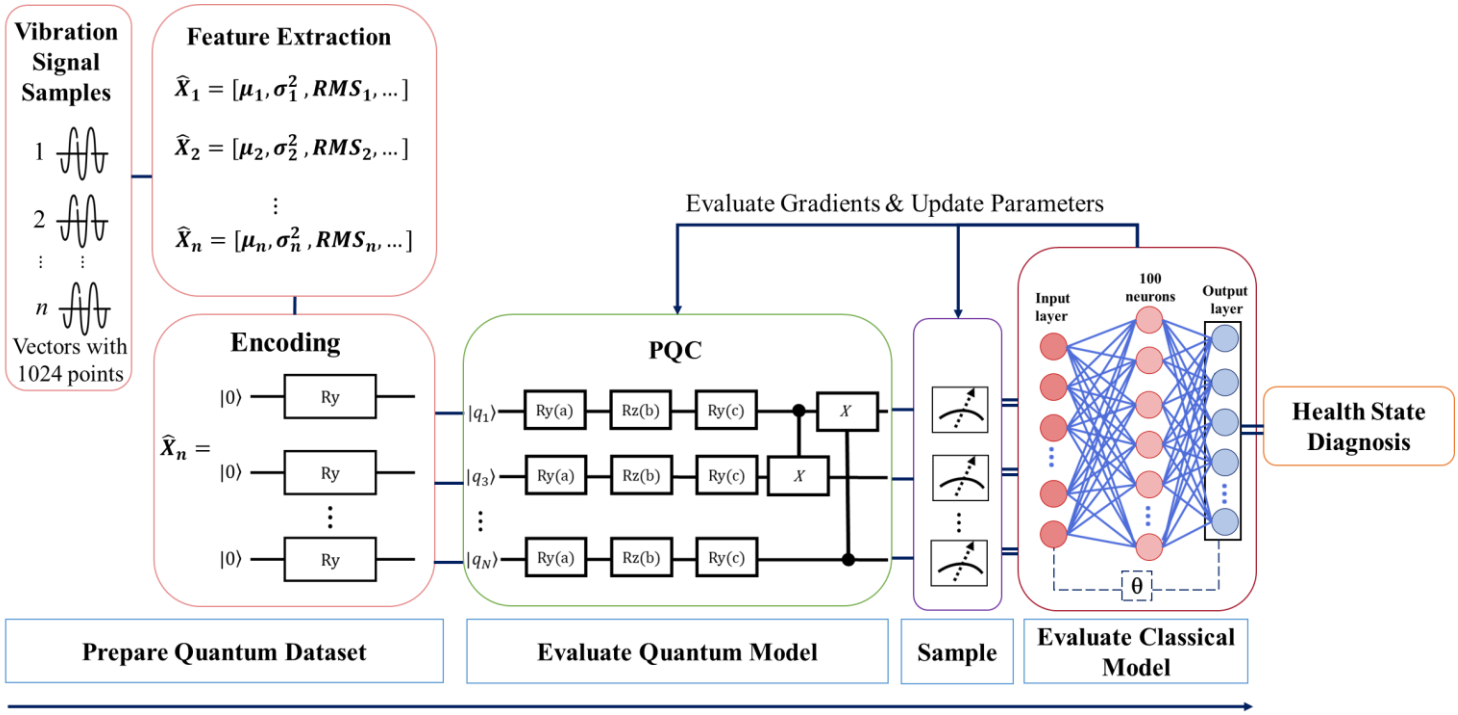

Source: The Author (2023).

Each stage is described below:

- Prepare Quantum Dataset: consists of pre-processing the classical data. For example, normalization, and feature extraction can be performed. $\widehat{X_1}, \widehat{X_2}, \ldots, \widehat{X_n}$ are vectors or multidimensional matrices, with a certain number of features monitored. Then, the data is encoded into qubits. A circuit is generated which takes as input N qubits defined in a $|0\rangle$ state and an N-dimensional real-valued vector, whose values lie in a range (e.g., $[0,1]$). Encoding schemas are a hot active debated topic that straddles the line between quantum hardware and software (CORREA-JULLIAN *et al*., 2022). Various methods could be utilized, such as amplitude encoding and angle encoding. We employed angle encoding. The data processing capabilities of quantum neural networks can directly benefit from this encoding method. This encoding's key advantage is that it is extremely effective in terms of operations because, regardless of the many data values to be encoded, just a fixed number of parallel processes are required (SIERRA-SOSA; TELAHUN; ELMAGHRABY, 2020). Eq. (13) summarizes the angle enconding method, where $\otimes$ represents the tensor product between the vector spaces *S*:

$$\vec{x} \rightarrow |\psi\rangle = S(x_0) \otimes S(x_1) \otimes \cdots \otimes S(x_{N-1}) \tag{13}$$

In Eq. (13), *S* represents the following operation performed for each element of the classical vector:

$$S(x_i) = cos\left(\frac{\pi}{2} x_i\right)|0\rangle + sin\left(\frac{\pi}{2} x_i\right)|1\rangle \tag{14}$$

- Evaluate quantum model: after encoding the data, PQC is created. PQC consists of one or several logic gates where the parameters of the gates (e.g., an angle θ of a rotation Y) are free parameters to be adjusted/optimized depending on the error propagated from outside to inside the circuit. In this study, we tested different PQC schemes. The first one consists only of rotation gates over y, x, and z, for each qubit (q_i), as shown in Figure 9. Note that *a*, *b*, and *c* are the angles of each gate to be parameterized.

Figure 9 – PQC defined by y, x and z rotation gates.

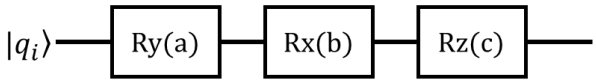

Source: The Author (2023).

In addition, we considered the circuit configuration used in the VQE quantum algorithm based on the study by Rasmussen and Zinner (2022). First, a Euler rotation is performed on each qubit, i.e., a combination of rotations in *y*, *z* and *y*, followed by a nearest-neighbor qubit coupling using the given entangling gate. Here, we apply the two-qubit gates CNOT, CZ, and *i*SWAP as shown in Figure 10. PQCs were built with different numbers of layers, namely, 1, 5, and 10. The maximum number of layers was 10 due to computational limitations. Above that, the processing of the models became too heavy for the simulator.

Figure 10 – PQC defined VQE with generic two-qubit gates visualization that in this study can be CNOT, CZ, or iSWAP.

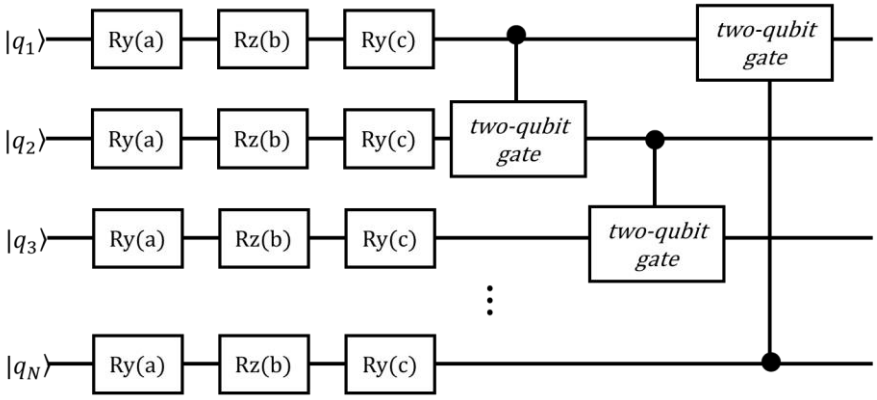

Source: The Author (2023).

- Sample or Average: measurements are performed, returning the processed quantum data to classical data. For this work, a measurement operation was defined through the Pauli Z-gate (Eq. (15)) in each of the qubits. Pauli measurements are a generalization of computational basis measurements that cover measurements in other bases and of equality between several qubits. A measurement in the Pauli Z basis projects the state onto one of the eigenstates $|0\rangle$ or $|1\rangle$ of this matrix (NIELSEN; CHUANG, 2010):

$$Z = \begin{bmatrix} 1 & 0 \\ 0 & -1 \end{bmatrix} \tag{15}$$

- Evaluate classical model: it collects the built features that are fed to the neural network. The error is calculated, as well as backpropagation of the error is performed through the gradients. The latter flow through the classical neural network weights and through PQC. At this stage, the diagnosis will be performed.

3.4 FEATURE EXTRACTION

Standard vibration-based metrics like mean, variance, root mean square (RMS), kurtosis, as well as higher order statistics, are frequently employed for machinery diagnostics (KIM *et al*., 2021; LYBECK; MARBLE; MORTON, 2007; MAIOR; MOURA; LINS, 2019; YE; YU, 2021). In this study, we will use eight different features. At first, five of them will be considered (mean, variance, RMS, peak-to-peak and maximum amplitude), as used in Silva and Droguett's (2022) study. Then, three more metrics will be added to observe if the results are improved or not, which are the Crest Factor, Kurtosis and Skewness. Since each feature corresponds to one qubit, our model then expanded from 5 to 8 qubits. Consequently, the circuit will have more replicas of the pre-defined logic gates that perform operations on these new quantum bits. Below these features will be defined:

- Variance and mean: the statistical dispersion of a signal is measured by variance (PERUCHI *et al*., 2020). The impacts in a spalled bearing should increase the signal's variability. The variance for a time series s_i with length L is:

$$\sigma^2 = \frac{1}{L}\sum_{i=1}^{L}(s_i - \bar{s})^2 \tag{16}$$

Where the population mean is:

$$\bar{s} = \frac{1}{L}\sum_{i=1}^{L} s_i \tag{17}$$

- RMS: it is the square root of the mean square, i.e., the arithmetic mean of the squares of the data. Also, it represents the residual signal energy, as shown in Eq. (18) (KIM *et al.*, 2021; LYBECK; MARBLE; MORTON, 2007):

$$RMS = \sqrt{\frac{1}{N}\sum_{i=1}^{N} x_i^2} \tag{18}$$

- Skewness: it describes a distortion or asymmetry in a set of data that departs from normal distribution. The curve is said to be skewed if it is displaced to the left or right.(ROSER *et al.*, 2020). It can be calculated as follows in Eq. (19) (NAYANA; GEETHANJALI, 2017):

$$SKW = \frac{\frac{1}{L}\sum_{i=1}^{L} |s_i - \bar{s}|^3}{\left(\sqrt{\frac{1}{L}\sum_{i=1}^{L} |s_i - \bar{s}|^2}\right)^3} \tag{19}$$

- Kurtosis: is frequently used as an indicator for quantifying vibration signal impulses (ANTONI; BORGHESANI, 2019). Kurtosis is a metric that can detect impulsive features in vibration signals and is directly related to vibration signal fault features (HEMMATI; ORFALI; GADALA, 2016; LI *et al.*, 2018). Kurtosis is defined as follows in Eq. (20):

$$Kurtosis = \frac{(L-1)\sum_{t-1}^{L}(s(t) - \bar{s})^4}{(\sum_{t-1}^{L}(s(s(t) - \bar{s}) - \bar{s})^2)^2} \tag{20}$$

- Peak-to-peak: is the difference between a waveform's maximum positive and maximum negative amplitudes (LYBECK; MARBLE; MORTON, 2007), and it is calculated according to Eq. (21):

$$PP = s_{max} - s_{min} \tag{21}$$

- Maximum Amplitude: is the maximum displacement or distance moved by a point on a vibrating body or wave measured from its equilibrium position (ZHANG; YANG, 2022). The notation for this feature is:

$$MaxAmp = s_{max} \tag{22}$$

- Crest Factor: is the ratio of the peak vibration level to the RMS and is frequently used to detect changes in signal patterns caused by impulse vibration sources that are not normally captured by RMS analysis alone. Under normal circumstances, its value ranges between 2 and 6. It is determined as follows:

$$Crest\ Factor = \frac{Peak\ Level}{RMS} \tag{23}$$

4 RESULTS

4.1 CWRU RESULTS

In the first data configuration developed for this study, five features were extracted from the time domain signal: (i) mean, (ii) variance, (iii) maximum amplitude, (iv) peak-to-peak, and (v) RMS. The second structure used the features from (i)-(v) and added the following: (vi) crest factor, (vii) kurtosis and (viii) skewness. The vibration signals were divided into segments of length equal to 1,024 points. The extension of the database resulted in 1,305 samples with the number of columns corresponding to the number of features.

The data was divided into 70% of its amount for training, while 30% was targeted for testing. Then, angle encoding was performed as described in the section 3.1. The output of this step are objects generated for reading and operation in the quantum circuits. These objects have a bijective relationship with the data points. That is, a data point has exactly one circuit representation. Figure 11 shows an example of a database vector with its respective encoding results.

Figure 11 - Vector with angle encoding.

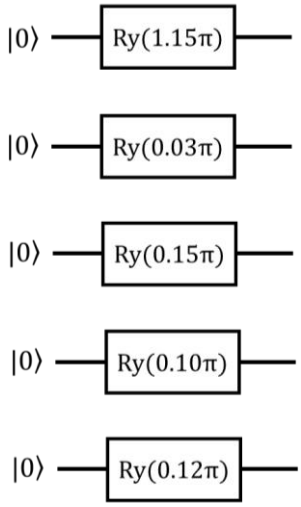

Source: The Author (2023).

In the end, the traditional neural network recieves as input the classical information obtained from the quantum measurement step. The processing was structured with three layers: the first one consists of the input units that depends of the number of the model features (5 or 8); the second has 100 neurons; and, finally, the output layer has the number of neurons

equivalent to the number of classes (10 and 12 to CWRU and JNU, respectively). The SoftMax activation function computes the scores for each class. Thus, the model provides the prediction of the corresponding failure mode. The cross-entropy categorical function is used to measure the models' losses. The default backpropagation operation of TFQ uses the finite difference method to compute the gradient approximation corresponding to the free parameters (rotation gates angles to parameterized: *a, b,* and *c*) (SILVA; DROGUETT, 2022). Adam optimizer (LIU *et al*., 2022) was used, with a learning rate of 0.01. We ran the training for 300 epochs, with the patience of 30 epochs for an early stop, i.e., the training ends if there is no improvement in the accuracy performance for 20 consecutive epochs (SARAYGORD AFSHARI *et al*., 2022). The above configuration is summarized in Table 4. For comparison purposes, the same structure was considered to represent the classical model (i.e., MLP).

Table 4 – Neural Network Setup.

Neural Network Setup	
Input Layer Neurons:	Nº of qubits (5 or 8)
Hiden Layer Neurons:	100
Ouput Layer Neurons:	Nº of classes (10 or 12)
Activation functions:	Relu, SoftMax
Loss function:	Cross entropy categorical
Optimizer:	Adam
Learning Rate:	0.01
Epochs:	300
Batch size:	32
Patience (Early Stop):	30

Source: The Author (2023).

Table 5 shows the accuracy, precision, recall, and F1-score results obtained when running the classic ML and QML models. Initially, the lowest accuracy presented is for MLP, resulting in 95.40% and 91.95% for five and eight features, respectively. Among the QML models with five features, the best accuracy (98.08%) is presented in three scenarios: only rotation gates with one layer; and VQE with the CZ gate having one and five circuit layers. However, observing the other metrics, the CZ with five layers had a better-weighted precision than the others.

Table 5 –CWRU: ML and QML Accuracy, Precision, Recall and F1-Score Results. Performances Change on a color Scale from shades of green for the best tesults, to red for the worst.

Category	Quantum gates	# of circuit layers	Accuracy (%)		Precision (%)		Recall (%)		F1-Score (%)	
			5 feat.	8 feat.	5 feat.	8 feat.	5 feat.	8 feat.	5 feat.	8 feat.
Classic ML (MLP)	-	-	95.40	91.95	96.06	92.88	95.40	91.95	95.20	91.48
QML	**Ry, Rx, Rz**	**1**	98.08	97.32	98.23	97.48	98.08	97.32	98.07	97.24
		5	96.93	95.02	97.38	95.34	96.93	95.02	96.84	94.88
		10	96.17	96.93	96.49	95.34	96.17	96.93	96.08	96.95
	VQE: Ry, Rz, Ry + CNOT	**1**	96.55	94.25	96.68	94.60	96.55	94.25	96.49	94.21
		5	96.17	95.02	96.68	95.27	96.17	95.02	96.02	95.03
		10	95.79	95.79	96.21	96.04	95.79	95.79	95.73	95.62
	VQE: Ry, Rz, Ry + CZ	**1**	98.08	96.93	98.21	97.23	98.08	96.93	98.02	96.90
		5	98.08	98.47	98.26	98.65	98.08	98.47	98.08	98.49
		10	96.17	96.55	96.70	96.83	96.17	96.55	96.20	96.47
	VQE: Ry, Rz, Ry + *i*SWAP	**1**	96.55	96.93	96.65	96.99	96.55	96.93	96.54	96.89
		5	96.55	95.79	96.61	96.10	96.55	95.79	96.49	95.72
		10	96.17	96.93	96.65	97.30	96.17	96.93	96.13	96.92

Source: The Author (2023).

Considering the first type of QML model (Ry, Rx, Rz), the behavior of the four metrics has better performances on circuits with only one layer and worse ones with ten layers. Thus, showing a decreasing pattern as the number of layers increases. The PQC with CNOT has the lowest accuracy of the QML models when applied to ten circuit layers (95.79%). Increasing this number to 10 peaks the performance to 96.55%. As observed, this result does not improve when increasing the number of layers. The PQC with CZ as the two-qubit gate has its worst result with ten layers and the best with 5 when considering mainly the precision. Finally, the *i*SWAP has similar behavior to CZ, i.e., the worst accuracy result for ten layers. However, best with one and intermediate with ten.

Still, in Table 5, we can observe the results for the model with eight features. In this scenario, MLP also has the worst accuracy (91.95%). The best result consists of the configuration of PQC with CZ and five layers (98.47%), which is approximately six percentage points greater than MLP. Results with eight features were better than those with five features in only six of the 13 configurations evaluated in this study.

Appendix A shows all the CWRU confusion matrices (CM) and accuracy curves. In the CMs, for the five features QML models with only rotation gates (Figure 12a), with CNOT (Figure 12b), and with CZ (Figure 12c), the most severe diagnostic problems were in label 2:

IR with 0.014 inches. The worst classification for *i*SWAP (Figure 12d), with one layer, was in label 5 (RE2).

Figure 12 - CWRU confusion matrices for 1-layer PQCs for the following configurations: (a) Ry, Rx, Rz; (b) Ry, Rz, Ry + CNOT; (c) Ry, Rz, Ry + CZ; (d) Ry, Rz, Ry + *i*SWAP.

(a) Ry, Rx, Rz

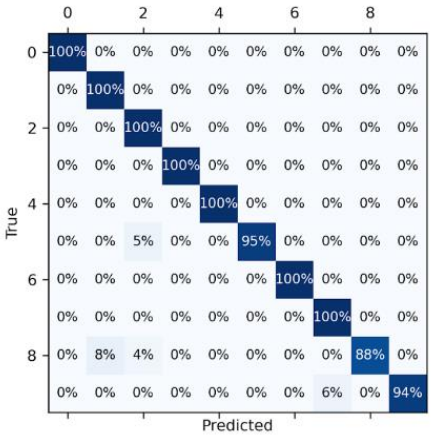

(b) Ry, Rz, Ry + CNOT

(c) Ry, Rz, Ry + CZ

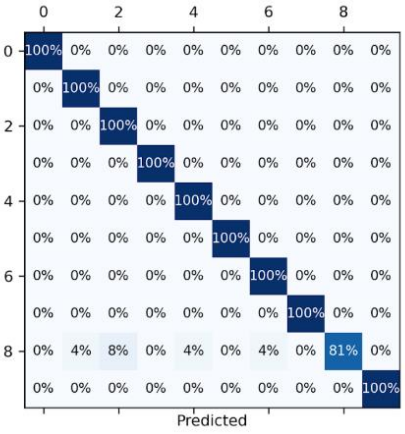

(d) Ry, Rz, Ry + *i*SWAP

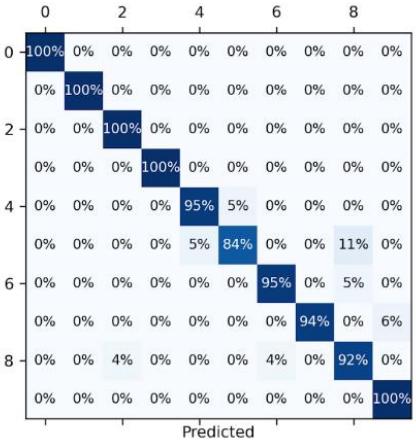

Source: The Author (2023).

The graphs of accuracy in Appendix A show the number of epochs for each model to achieve its best result, according to the stopping criterion used (patience of 30 epochs). Figure 13 summarizes some of these graphics. For the circuits with only one layer, one observes that the model with only rotations (Figure 13a) needed 48 epochs to reach its peak accuracy. The other configurations, on the other hand, varied around 80 epochs. In this case, CNOT with 81 (Figure 13b), CZ with 80 (Figure 13c), and *i*SWAP with 76 (Figure 13c). Regarding the circuit repetition, not necessarily more layers need more epochs, as it was not true for the four tested configurations.

Figure 13 - CWRU accuracy curves for 1-layer PQCs for the following configurations: (a) Ry, Rx, Rz; (b) Ry, Rz, Ry + CNOT; (c) Ry, Rz, Ry + CZ; (d) Ry, Rz, Ry + *i*SWAP

(a) Ry, Rx, Rz

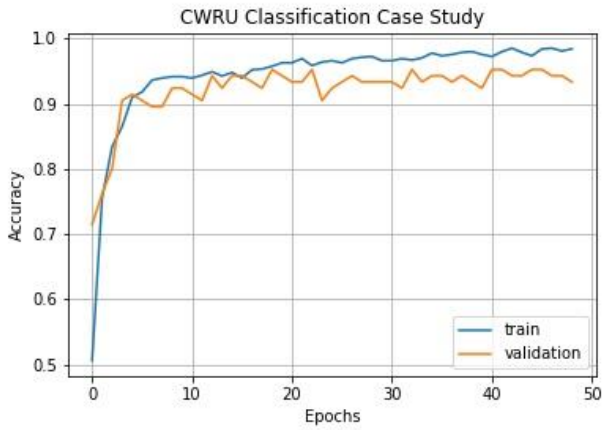

(b) Ry, Rz, Ry + CNOT

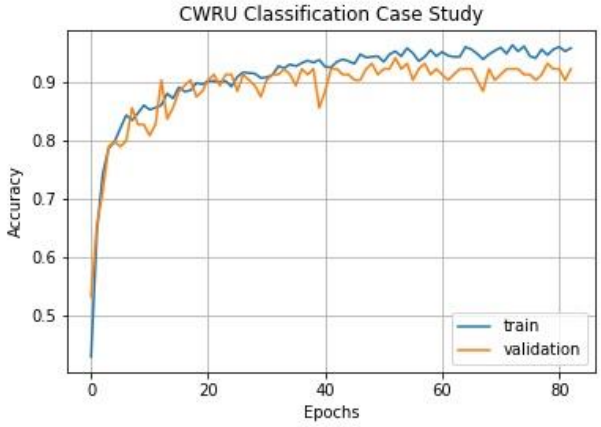

(c) Ry, Rz, Ry + CZ

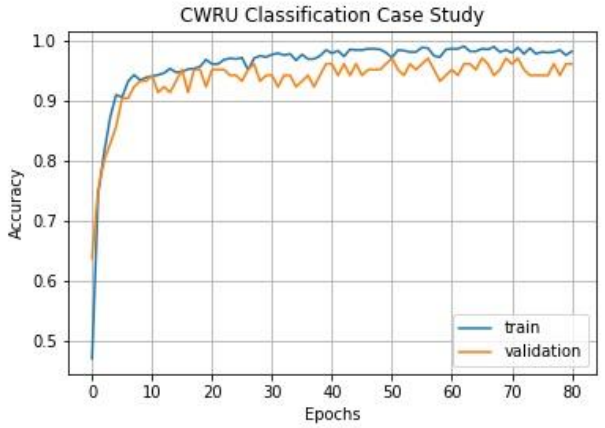

(d) Ry, Rz, Ry + *i*SWAP

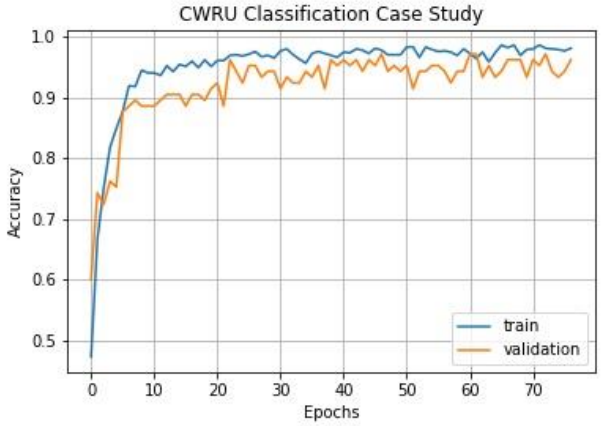

Source: The Author (2023).

4.1.1 CWRU Results considering Time and Frequency domain

In this section, the experiments were run with the proportions of 80% of samples as the training set and 20% of samples as the testing set which were randomly selected. We used both signals from time and from frequency domain with the same features used before. To obtain reliable results and show the best validation accuracy that the models can achieve, we repeat each experiment five times. Four indicators are used to assess the performance of models, including the mean and maximum values of the accuracy obtained by the last epoch and the mean and maximum values of the maximal accuracy. For simplicity, they can be denoted as Last-Mean, Last-Max, Best-Mean, and Best-Max, respectively. These metrics will be used with the aim to compare our results with those aquired by Zhao *et al*. (2020) using classical methods, such as, MLP, Convolutional Neural Network (CNN) and AutoEncoder (AE).

It is important to highlight that we used features extracted from the data, as explained in the methodology and results sections (respectively, 3.4 and 4.1), due to qubits limitations while Zhao *et al*. (2020) used the complete signal. Thus, using features some information may be lost during the training process. Also, the networks architectures are also different to more information about them see Zhao *et al*. (2020).

According to Table 6, most of the best results came from the configuration with data in the time domain with 8 features. Less so in the PQC architecture with VQE and CZ gate, where the best performances concern data in the frequency domain with 8 features. It is observed that the data tends to be better, regardless of the domain, with 8 qubits. Comparing the results with the classical models, it can be seen that Zhao *et al*. (2020) achieved 100% accuracy training when using CNN in both domains. With MLP and AE it achieved this mark only in the frequency domain. The QML configurations used in this work are shown to be superior to MLP and AE in the time domain. However, it is possible that the deep structure of the training influences the achievement of an accuracy rating of 100%.

Table 6 – CWRU: Comparison between QML from this study and Classic DL from Zhao *et al*. (2020) results

Category	**Quantum gates**	**# of layers**	**Metric**	**Time Domain**		**Frequency Domain**	
				Accuracy (%)		**Accuracy (%)**	
				5 features	**8 features**	**5 features**	**8 features**
QML	Ry, Rx, Rz	1	Last Mean	94.10	**96.76**	94.10	95.24
			Best Mean	96.38	**98.48**	96.57	98.10
			Last Max	96.19	**98.10**	94.29	97.14
			Best Max	98.10	**99.05**	97.14	99.05
		5	Last Mean	92.38	**96.76**	94.29	95.81
			Best Mean	94.29	**98.48**	96.95	97.52
			Last Max	97.14	**98.10**	96.19	97.14
			Best Max	98.10	**99.05**	98.10	98.10
		10	Last Mean	92.00	95.24	91.24	**95.62**
			Best Mean	93.90	**97.90**	96.57	**97.90**
			Last Max	**97.14**	**97.14**	96.19	99.05
			Best Max	98.10	**99.05**	97.14	**99.05**
	VQE: Ry, Rz, Ry + CNOT	1	Last Mean	90.48	**91.81**	82.86	88.19
			Best Mean	**93.33**	93.14	86.29	90.48
			Last Max	**95.24**	93.33	89.52	92.38
			Best Max	**96.19**	95.24	93.33	92.38
		5	Last Mean	93.71	**94.67**	92.57	90.67
			Best Mean	95.24	96.38	95.62	93.90
			Last Max	96.19	**97.14**	95.24	95.24
			Best Max	**97.14**	**97.14**	96.19	95.24

		10	Last Mean	92.00	**92.57**	91.43	88.76
			Best Mean	95.24	**95.81**	94.29	91.62
			Last Max	**95.24**	93.33	**95.24**	92.38
			Best Max	**98.10**	96.19	95.24	94.29
	VQE: Ry, Rz, Ry + CZ	1	Last Mean	94.67	95.24	89.71	**96.00**
			Best Mean	96.95	96.76	92.00	**97.33**
			Last Max	96.19	97.14	96.19	**99.05**
			Best Max	98.10	98.10	97.14	**99.05**
		5	Last Mean	94.48	**96.00**	91.05	94.67
			Best Mean	96.38	**97.52**	95.43	97.33
			Last Max	97.14	**98.10**	94.29	97.14
			Best Max	98.10	**99.05**	97.14	98.10
		10	Last Mean	93.90	**94.29**	90.86	92.00
			Best Mean	95.43	**96.57**	92.95	95.24
			Last Max	96.19	94.14	94.29	93.33
			Best Max	97.14	**98.10**	95.24	97.14
	VQE: Ry, Rz, Ry + *i*SWAP	1	Last Mean	**95.81**	94.29	89.90	95.24
			Best Mean	**97.71**	97.52	94.67	**97.71**
			Last Max	96.19	**97.14**	93.33	96.19
			Best Max	98.10	**99.05**	97.14	98.10
		5	Last Mean	**94.10**	**94.10**	93.52	92.95
			Best Mean	96.38	**96.76**	95.24	96.00
			Last Max	95.24	95.24	**98.10**	96.19
			Best Max	98.10	**99.05**	98.10	98.10
		10	Last Mean	94.86	94.10	91.43	90.86
			Best Mean	95.81	**96.19**	95.62	95.62
			Last Max	**96.19**	95.24	95.24	95.24
			Best Max	96.19	**98.10**	97.14	**98.10**
Classical ML (ZHAO *et al.*., 2020)	**Model**		**Metric**	**Time Domain**		**Frequency Domain**	
	MLP	-	Last Mean	60.00		**100**	
		-	Best Mean	61.72		**100**	
		-	Last Max	62.24		**100**	
		-	Best Max	63.02		**100**	
	CNN	-	Last Mean	99.58		**99.89**	
		-	Best Mean	99.79		**99.92**	
		-	Last Max	**100**		**100**	
		-	Best Max	**100**		**100**	
	AE	-	Last Mean	54.71		100	
		-	Best Mean	71.42		100	
		-	Last Max	66.67		100	
		-	Best Max	73.95		100	

Source: The Author (2023).

The trainable parameters of the models can also be compared. In this study, the classic MLP model has 1,610 and 1,910 trainable parameters for 5 and 8 features, respectively. On the other hand, the QML models have three more trainable parameters that correspond to the angles of the PQC rotation gates. Thus, the models with quantum components have a total of 1,613 and 1,913 trainable parameters for the respective input types of 5 and 8 features. In comparison, the models of Zhao *et al*. (2020) have higher numbers of trainable parameters. Their simplest DL framework, the deep MLP, composed of five fully connected layers and five corresponding batch normalization layers, has 695,146 trainable parameters. Thus, the models employed in this research were competitive to a degree comparable to approximately 0.23% of the parameter quantity utilized in the deep MLP of Zhao *et al*. (2020). The more complex AE and CNN also have even larger numbers of trainable parameters than MLP. Therefore, it can be concluded that the models used in this study are less computationally expensive in terms of trainable parameters.

4.2 JNU RESULTS

The settings used for training this database are similar to those of the CWRU. However, this is a larger database that resulted in a sample size of 8,790 rows and 12 health states. Indeed, JNU is a more complex database than CWRU. In a study dealing with seven different databases from the rotating machinery components literature, the authors state that JNU is at 3 out of 4 levels of difficulty, while CWRU is at 1 out of 4 (see Zhao *et al*., 2020).

Table 7 presents the accuracy, precision, recall, and F1-score results obtained from the Classic MLP and QML models. With five features, the lowest accuracy was obtained for the MLP, resulting in 61.59% of the test data, followed by VQE with CZ with ten layers (62.19%). The best accuracy was in the PQC with the two-qubit gate CZ and one-layer circuit with an accuracy of 70.49%, followed by rotation gates and with *i*SWAP, both with one layer, that hit 70.31% and 70.27%, respectively. However, when we look at the precision metric, the order of best performance goes first to *i*SWAP (68.63%), then to VQE with CZ (67.74%), and lastly to just rotation gates (67.70%). For all metrics, the model with the CNOT two-qubit gate is the only one with just intermediate to low values since it does not have any green highlights in Table 7.

Table 7 – JNU: ML and QML Accuracy, Precision, Recall and f1-score results. performances change on a color scale from shades of green for the best tesults, to red for the worst.

Category	Quantum gates	# of circuit layers	Accuracy (%)		Precision (%)		Recall (%)		F1-Score (%)	
			5 feat.	8 feat.	5 feat.	8 feat.	5 feat.	8 feat.	5 feat.	8 feat.
Classic ML (MLP)	-	-	61.59	62.57	49.91	56.52	61.59	62.57	53.91	56.11
QML	**Ry, Rx, Rz**	**1**	70.31	70.04	67.70	67.98	70.31	70.04	68.29	68.08
		5	69.28	69.93	65.47	68.06	69.28	69.93	65.38	67.78
		10	68.49	68.37	65.72	66.10	68.49	68.37	65.91	65.80
	VQE: Ry, Rz, Ry + CNOT	**1**	63.41	63.44	58.94	58.07	63.41	63.44	57.98	58.37
		5	66.02	65.91	62.13	62.52	66.02	65.91	62.76	61.55
		10	65.19	67.90	61.52	63.93	65.19	67.80	60.68	64.26
	VQE: Ry, Rz, Ry + CZ	**1**	70.42	68.37	67.74	65.70	70.42	68.37	67.67	65.69
		5	64.88	67.80	59.95	64.41	64.88	67.80	59.88	64.75
		10	62.19	68.41	57.43	65.09	62.19	68.41	58.19	65.58
	VQE: Ry, Rz, Ry + *i*SWAP	**1**	70.27	70.19	68.63	67.47	70.27	70.19	67.67	67.98
		5	69.43	67.65	65.89	64.22	69.43	67.65	66.62	63.65
		10	64.92	64.85	59.33	61.89	64.92	64.85	60.42	61.64

Source: The author (2023).

With eight features, the worst accuracy was obtained by the same configuration of five features: MLP (62.57%). The second place belongs to the VQE with CNOT with one layer (63.44%). The other metrics follow the same order. The best accuracy was obtained with the *i*SWAP (one layer) with an accuracy of 70.19%, followed by rotation gates (Ry, Rx, Rz) with one and five layers, corresponding to 70.04% and 69.93%, respectively. However, the accuracy of rotation gates with five layers (68.06%) is better than rotation gates with one layer and *i*SWAP (one layer). The latter two configurations have accuracy in the order previously written, with 67.98% and 67.47%, respectively.

Note that the best precision is approximately 11 percentage points greater than the Classic MLP. In addition, with eight features, increasing metrics performance behavior by adding the layers only happened in the configuration with CNOT.

Appendix B presents the JNU confusion matrices and accuracy curves. Concerning the CMs, for the five features QML models with only rotation gates (Figure 14a) and *i*SWAP (Figure 14d), both with one layer, the most severe diagnostic problems were in label 7: rolling Element 2 at 800 rpm. For CNOT (Figure 14b) and CZ (Figure 14c), it was, respectively, label 4 (inner ring at 800 rpm) and label 3 (rolling element at 600 rpm).

Figure 14 - JNU confusion matrices for 1-layer PQCs for the following configurations: (a) Ry, Rx, Rz; (b) Ry, Rz, Ry + CNOT; (c) Ry, Rz, Ry + CZ; (d) Ry, Rz, Ry + *i*SWAP.

(a) Ry, Rx, Rz

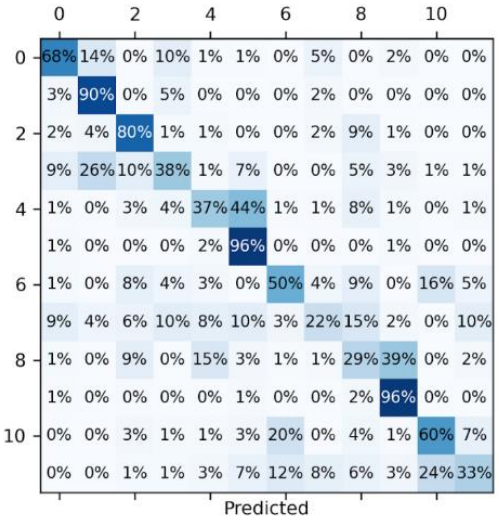

(b) Ry, Rz, Ry + CNOT

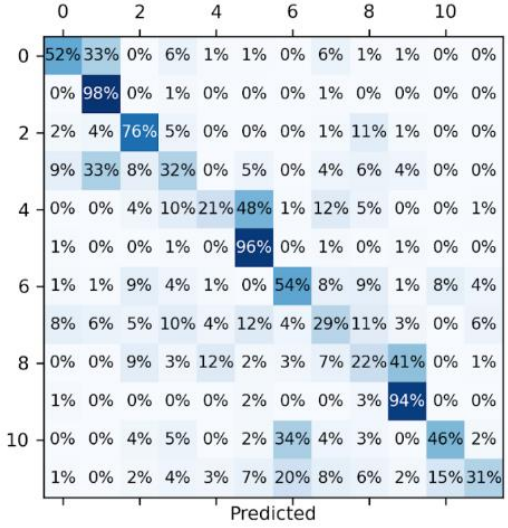

(c) Ry, Rz, Ry + CZ

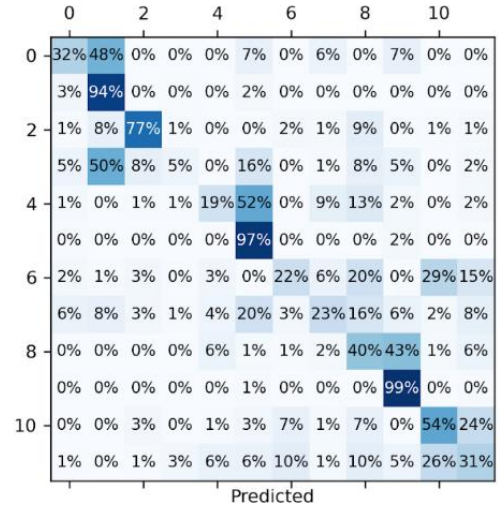

(d) Ry, Rz, Ry + *i*SWAP

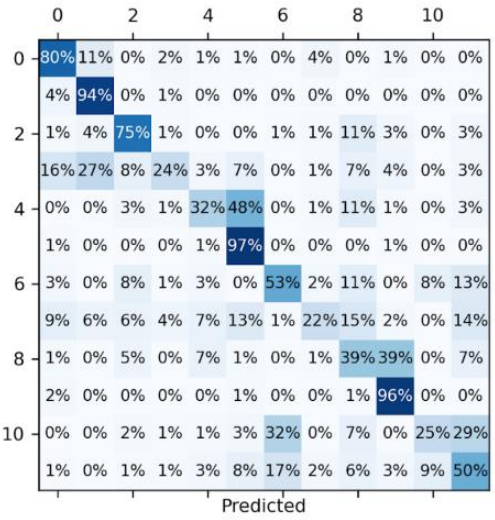

Source: The author (2023).

The accuracy graphs in Appendix B display the number of epochs required by each model to produce its best outcome. The more layers in PQCs using iSWAP (Figure 15d), the more epochs are required. However, for only rotation gates (Figure 15a), VQE with CNOT (Figure 15b), and VQE with CZ (Figure 15c), we did not observe such a behavior.

Figure 15 - JNU accuracy curves for 1-layer PQCs for the following configurations: (a) Ry, Rx, Rz; (b) Ry, Rz, Ry + CNOT; (c) Ry, Rz, Ry + CZ; (d) Ry, Rz, Ry + *i*SWAP

(a) Ry, Rx, Rz

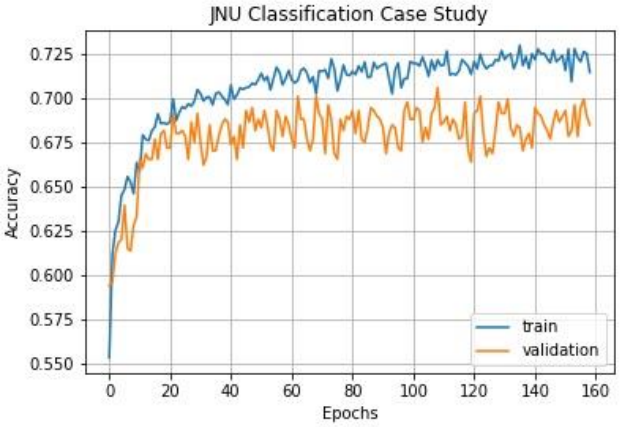

(b) Ry, Rx, Rz + CNOT

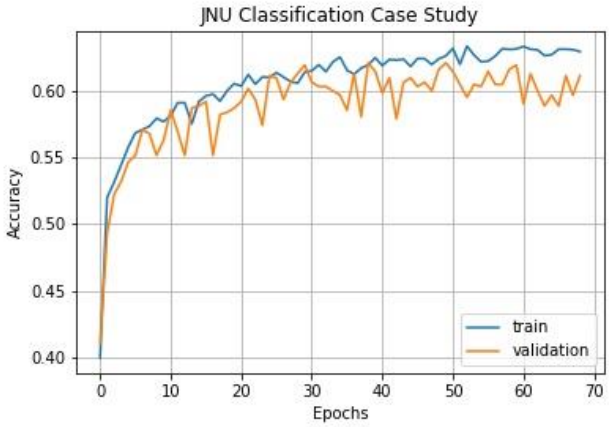

(c) Ry, Rx, Rz + CZ

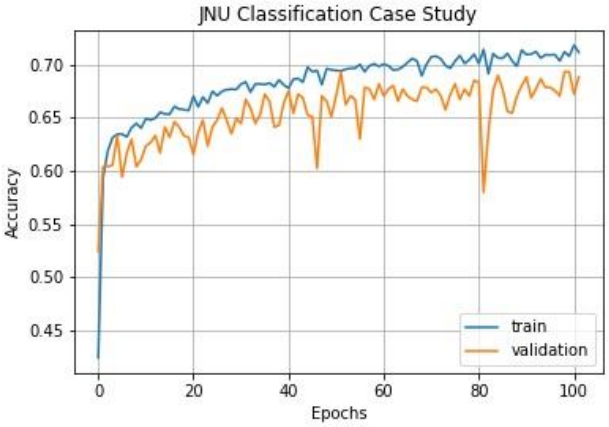

(d) Ry, Rx, Rz + *i*SWAP

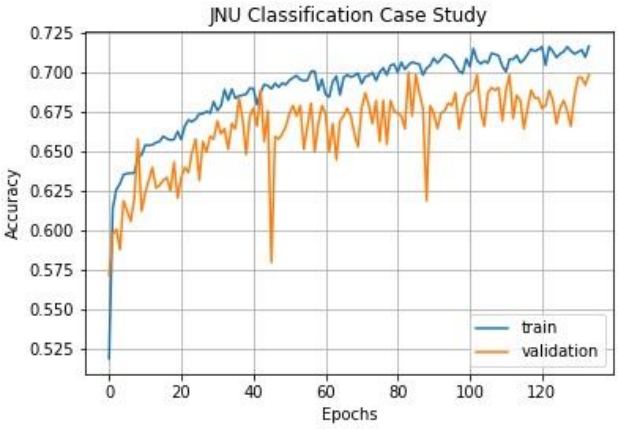

Source: The Author (2023).

4.2.1 JNU Results considering Time and Frequency domains

In this section, the analysis will be done according to the settings explained in section 4.1.1. Table 8 shows the results with time and frequency domain. Note that time domain just has outputs with 5 features due to the longer time to run the model. Regarding in a general way, the time domain with 5 features presented the best scores. They are also greater than those indicated by Zhao *et al*. (2020) in the MLP and AE models. However, as in CWRU, CNN was better in both domains. It is important to recall that Zhao *et al*. (2020) applied models trained through with the complete signal. This may have led to CNN's improved performance.

Table 8 – JNU: Comparison between QML from this study and Classic DL from Zhao *et al*. (2020) results

Category	Quantum gates	# of layers	Metric	Time Domain	Frequency Domain	
				Accuracy (%)	Accuracy (%)	
				5 features	5 features	8 features
QML	Ry, Rx, Rz	1	Last Mean	**67.21**	62.82	62.95
			Best Mean	**68.54**	64.19	64.51
			Last Max	**68.83**	63.63	63.47
			Best Max	**67.21**	64.61	65.10
		5	Last Mean	**64.58**	62.14	62.63
			Best Mean	**68.08**	64.42	65.03
			Last Max	**66.88**	63.80	64.45
			Best Max	**69.16**	64.77	65.75
		10	Last Mean	**66.59**	62.63	60.45
			Best Mean	**68.02**	64.45	64.54
			Last Max	**68.51**	63.64	63.47
			Best Max	**69.48**	65.26	65.10
	VQE: Ry, Rx, Rz + CNOT	1	Last Mean	**61.01**	59.61	60.16
			Best Mean	**63.08**	61.40	61.82
			Last Max	62.50	60.55	**62.99**
			Best Max	**63.96**	63.15	62.99
		5	Last Mean	**64.03**	60.49	61.49
			Best Mean	**65.75**	63.21	63.70
			Last Max	**65.42**	61.69	62.82
			Best Max	**66.56**	63.80	64.29
		10	Last Mean	61.56	60.75	**62.66**
			Best Mean	**65.62**	63.02	63.70
			Last Max	**65.26**	62.18	65.10
			Best Max	**67.21**	64.12	65.10
	VQE: Ry, Rx, Rz + CZ	1	Last Mean	**67.24**	62.34	63.05
			Best Mean	**68.54**	63.15	64.74
			Last Max	**68.34**	64.29	63.63
			Best Max	**69.32**	65.26	65.10
		5	Last Mean	**63.77**	62.66	61.20
			Best Mean	**67.53**	64.16	63.12
			Last Max	**68.02**	63.96	62.82
			Best Max	**70.62**	65.10	65.09
		10	Last Mean	**63.54**	61.88	61.10
			Best Mean	**65.91**	63.70	63.90
			Last Max	**65.10**	63.80	65.10
			Best Max	**67.86**	64.45	65.10
	VQE: Ry, Rx, Rz + *i*SWAP	1	Last Mean	**67.24**	62.14	62.56
			Best Mean	**68.28**	64.48	64.61
			Last Max	**68.51**	63.31	63.31
			Best Max	**69.48**	65.10	64.94

		5	Last Mean	**64.29**	61.49	62.01
			Best Mean	**67.11**	62.89	64.61
			Last Max	**67.69**	64.12	63.63
			Best Max	**68.02**	64.61	64.61
		10	Last Mean	**64.68**	62.89	62.05
			Best Mean	**66.56**	63.99	63.54
			Last Max	**66.23**	63.80	63.80
			Best Max	**68.34**	64.94	64.12
Classical ML	**Model**		**Metric**	**Time Domain**	**Frequency Domain**	
	MLP	-	Last Mean	40.60	**96.52**	
		-	Best Mean	45.17	**97.44**	
		-	Last Max	44.94	**97.21**	
		-	Best Max	46.25	**97.78**	
	CNN	-	Last Mean	80.79	**92.88**	
		-	Best Mean	83.56	**94.01**	
		-	Last Max	82.31	**94.25**	
		-	Best Max	84.81	**94.60**	
	AE	-	Last Mean	41.64	**95.77**	
		-	Best Mean	44.68	**96.78**	
		-	Last Max	45.11	**96.47**	
		-	Best Max	45.96	**96.99**	

Source: The author (2023).

The number of trainable parameters for the QML models with 5 and 8 features in this database are 1,815 and 2,115, respectively. Meanwhile, the classic MLP model used in this study has 1,812 and 2,112 trainable parameters, which is 3 fewer parameters than the QML models. In contrast, Zhao *et al.*'s (2020) deep MLP, composed of five fully connected layers and five corresponding batch normalization layers, has 746,408 trainable parameters, which is significantly more computationally expensive than the models used in this research - corresponding to only 0.24% of those used by the authors mentioned above.

4.3 DISCUSSION

Here we outline more general considerations of the obtained results presented for each database regarding the trained structures. Note that we base our observations on the content of Tables 5 and 7.

We varied our models in three aspects: (1) the number of features; (2) PQC quantum operations structure; and (3) the number of circuit layers. In (1), since the quantum simulator used cannot process the complete signal, given the limitation of qubits, extracting features is a

way to test the QC models. We use these two types of inputs, 5 and 8 features, to infer if a larger amount would yield better metric results.

In the classical model (MLP), different behaviors occurred in the two databases: the results with five features were better in all metrics for CWRU, while in JNU, it was the opposite. For the quantum models, on the other hand, this varied. In the CWRU, when considering the precision metric, the results with five features were better than the eight features' results since they were successful in 58.33% of the cases. For JNU, in turn, results with eight features were the ones that obtained this percentage. But when observing the recall, for example, in CWRU, in six out of 12 scenarios, the results with eight features were better, and in one of them, the results were equal. In JNU, five features came out on top, with seven out of 12 results.

We performed the Mann-Whitney statistical test for two independent random samples (MONTGOMERY; RUNGER, 2010) to evaluate the hypothesis that the medians of the balanced accuracies of the two populations (5 and 8 features) are equal by model configuration. We executed 10 training rounds for each of the Classic ML and QML models, resulting in a total of 130 balanced accuracy values for each input size (either five feature or eight features), as shown in Table 9 and Table 10.

Table 9 – CWRU: Balanced accuracy samples of the models by features.

Model	Features	Balanced Accuracy
MLP	5	[0.9109, 0.9490, 0.9507, 0.9535, 0.9563, 0.9563, 0.9469, 0.9601, 0.9546, 0.9640]
	8	[0.9170, 0.9418, 0.9465, 0.9521, 0.9501, 0.9521, 0.9587, 0.9587, 0.9587, 0.9587]
Ry, Rx, Rz (1 layer)	5	[0.9577, 0.9599, 0.9613, 0.9703, 0.9748, 0.9782, 0.9654, 0.9787, 0.9717, 0.9762]
	8	[0.9752, 0.9650, 0.9717, 0.9762, 0.9370, 0.9640, 0.9689, 0.9801, 0.9563, 0.9570]
Ry, Rx, Rz (5 layers)	5	[0.9750, 0.9586, 0.9455, 0.9725, 0.9350, 0.9923, 0.9337, 0.9731, 0.9878, 0.9612]
	8	[0.9653, 0.9191, 0.9710, 0.9846, 0.9794, 0.9813, 0.9846, 0.9832, 0.9658, 0.9820]
Ry, Rx, Rz (10 layers)	5	[0.9832, 0.9832, 0.9624, 0.9885, 0.9538, 0.9711, 0.9515, 0.9599, 0.9613, 0.9391]
	8	[0.9666, 0.9717, 0.9717, 0.9962, 0.9565, 0.9170, 0.9717, 0.9759, 0.9762, 0.9237]
VQE: Ry, Rz, Ry + CNOT (1 layer)	5	[0.9142, 0.8844, 0.9443, 0.9001, 0.9219, 0.9252, 0.9377, 0.9381, 0.8930, 0.8935]
	8	[0.9300, 0.9085, 0.9273, 0.9198, 0.9176, 0.9191, 0.9288, 0.9041, 0.9353, 0.9293]
VQE: Ry, Rz, Ry + CNOT (5 layers)	5	[0.9638, 0.9792, 0.9689, 0.9724, 0.9679, 0.9719, 0.9413, 0.9585, 0.9281, 0.9397]
	8	[0.9499, 0.9648, 0.9364, 0.9773, 0.9309, 0.9510, 0.9478, 0.9611, 0.9604, 0.9223]

VQE: Ry, Rz, Ry + CNOT (10 layers)	5	[0.9687, 0.9296, 0.9547, 0.9468, 0.9662, 0.9346, 0.9679, 0.9414, 0.9640, 0.9638]
	8	[0.9659, 0.9736, 0.9669, 0.9508, 0.9501, 0.8812, 0.9674, 0.9653, 0.9443, 0.9870]
VQE: Ry, Rz, Ry + CZ (1 layer)	5	[0.9668, 0.9884, 0.9770, 0.9252, 0.9500, 0.9409, 0.9621, 0.9727, 0.9546, 0.9846]
	8	[0.9799, 0.9794, 0.9762, 0.9716, 0.9808, 0.9671, 0.9710, 0.9658, 0.9717, 0.9559]
VQE: Ry, Rz, Ry + CZ (5 layers)	5	[0.9571, 0.9617, 0.9503, 0.9741, 0.9283, 0.9830, 0.9316, 0.9509, 0.9762, 0.9685]
	8	[0.9365, 0.9606, 0.9662, 0.9610, 0.9435, 0.9611, 0.9813, 0.9863, 0.9624, 0.9762]
VQE: Ry, Rz, Ry + CZ (10 layers)	5	[0.9315, 0.9634, 0.9147, 0.9407, 0.9299, 0.9399, 0.9480, 0.9612, 0.9721, 0.9583]
	8	[0.9549, 0.9606, 0.9717, 0.9381, 0.9664, 0.9434, 0.9678, 0.9623, 0.9510, 0.9621]
VQE: Ry, Rz, Ry + *i*SWAP (1 layer)	5	[0.9832, 0.9832, 0.9830, 0.9832, 0.9832, 0.9453, 0.9769, 0.9587, 0.9752, 0.9345]
	8	[0.9479, 0.9878, 0.9489, 0.9595, 0.9846, 0.9468, 0.9685, 0.9614, 0.9769, 0.9413]
VQE: Ry, Rz, Ry + *i*SWAP (5 layers)	5	[0.9500, 0.9531, 0.9660, 0.9747, 0.9507, 0.9745, 0.9595, 0.9787, 0.9753, 0.9540]
	8	[0.9320, 0.9616, 0.9350, 0.9748, 0.9760, 0.9589, 0.9380, 0.9369, 0.9456, 0.9678]
VQE: Ry, Rz, Ry + *i*SWAP (10 layers)	5	[0.9792, 0.9365, 0.9498, 0.9566, 0.9474, 0.9547, 0.9422, 0.9678, 0.9520, 0.9490]
	8	[0.9458, 0.9557, 0.9467, 0.9878, 0.9519, 0.9486, 0.9414, 0.9416, 0.9608, 0.9573]

Source: The Author (2023).

Table 10 – JNU: Balanced accuracy samples of the models by features.

Model	Features	Balanced Accuracy
MLP	5	[0.4339, 0.4523, 0.4642, 0.4982, 0.5046, 0.5250, 0.5211, 0.5311, 0.5252, 0.5292]
	8	[0.4684, 0.4668, 0.4817, 0.4870, 0.5198, 0.5183, 0.5323, 0.5256, 0.5254, 0.5314]
Ry, Rx, Rz (1 layer)	5	[0.5588, 0.5781, 0.5796, 0.5614, 0.5654, 0.5678, 0.5743, 0.5764, 0.5668, 0.5528]
	8	[0.5835, 0.5707, 0.5779, 0.5831, 0.5789, 0.5777, 0.5799, 0.5703, 0.5833, 0.5770]
Ry, Rx, Rz (5 layers)	5	[0.5105, 0.5520, 0.5579, 0.5564, 0.5681, 0.5572, 0.5707, 0.5599, 0.5809, 0.4765]
	8	[0.5768, 0.5703, 0.5706, 0.5332, 0.5680, 0.5710, 0.5740, 0.5660, 0.5821, 0.5801]
Ry, Rx, Rz (10 layers)	5	[0.5407, 0.5088, 0.5664, 0.5612, 0.5670, 0.5079, 0.5601, 0.5201, 0.4927, 0.5572]
	8	[0.5276, 0.5820, 0.4667, 0.5095, 0.5783, 0.5778, 0.5693, 0.5746, 0.5596, 0.5510]
VQE: Ry, Rz, Ry + CNOT (1 layer)	5	[0.4633, 0.4862, 0.4567, 0.4664, 0.4693, 0.4818, 0.4541, 0.4859, 0.4600, 0.4743]
	8	[0.4730, 0.4387, 0.4840, 0.4684, 0.4009, 0.4503, 0.4567, 0.4718, 0.4725, 0.4520]
VQE: Ry, Rz, Ry + CNOT (5 layers)	5	[0.5066, 0.5360, 0.5277, 0.5176, 0.5081, 0.5001, 0.5148, 0.5059, 0.4727, 0.4767]
	8	[0.4992, 0.5022, 0.5126, 0.5248, 0.5187, 0.4878, 0.5533, 0.5072, 0.5191, 0.5435]
VQE: Ry, Rz, Ry + CNOT (10 layers)	5	[0.4603, 0.4907, 0.4906, 0.5030, 0.4901, 0.4996, 0.4995, 0.5141, 0.4913, 0.4941]
	8	[0.5275, 0.5036, 0.4863, 0.5102, 0.5094, 0.5104, 0.5009, 0.4743, 0.5233, 0.4926]
VQE: Ry, Rz, Ry + CZ (1 layer)	5	[0.5613, 0.5679, 0.5774, 0.5706, 0.5717, 0.5690, 0.5576, 0.5775, 0.5748, 0.5560]
	8	[0.5715, 0.5786, 0.5549, 0.5866, 0.5749, 0.5692, 0.5777, 0.5721, 0.5792, 0.5816]
VQE: Ry, Rz, Ry + CZ (5 layers)	5	[0.5009, 0.5371, 0.5560, 0.5131, 0.5240, 0.5698, 0.5121, 0.5581, 0.5487, 0.4886]
	8	[0.5263, 0.5161, 0.5654, 0.5277, 0.5876, 0.5108, 0.5263, 0.5088, 0.5175, 0.5517]
VQE: Ry, Rz, Ry + CZ (10 layers)	5	[0.5032, 0.4967, 0.5202, 0.5113, 0.4861, 0.5256, 0.5171, 0.4323, 0.5041, 0.5183]
	8	[0.5105, 0.5480, 0.5615, 0.5333, 0.5321, 0.5274, 0.5162, 0.5347, 0.5392, 0.5594]
VQE: Ry, Rz, Ry + *i*SWAP (1 layer)	5	[0.5640, 0.5747, 0.5807, 0.5745, 0.5589, 0.5564, 0.5663, 0.5710, 0.5765, 0.5520]
	8	[0.5670, 0.5745, 0.5778, 0.5826, 0.5863, 0.5677, 0.5799, 0.5710, 0.5722, 0.5738]
VQE: Ry, Rz, Ry + *i*SWAP (5 layers)	5	[0.5019, 0.5277, 0.5451, 0.5121, 0.5636, 0.5349, 0.4567, 0.4905, 0.5362, 0.5181]
	8	[0.5148, 0.5225, 0.5657, 0.5321, 0.5624, 0.5521, 0.5170, 0.4572, 0.5240, 0.5071]
VQE: Ry, Rz, Ry + *i*SWAP (10 layers)	5	[0.5231, 0.5124, 0.5004, 0.4890, 0.4993, 0.5017, 0.5486, 0.4714, 0.5222, 0.5207]
	8	[0.5135, 0.5124, 0.5513, 0.5237, 0.4966, 0.5075, 0.5346, 0.5128, 0.5132, 0.5525]

For the execution of the statistical test, we set the following hypotheses: H_0 – No difference between the balanced accuracy medians when related to the factor "number of features"; H_1: the two balanced accuracy medians are different when related to the factor "number of features". The significance level defined for this case was 0.05 (for more information about Mann-Whitney test calculation see Montgomery and Runger (2010)). According to Table 11, for each of the CWRU models we cannot reject the null hypothesis that the two medians are different. However, for JNU, statistical evidence for rejecting H_0 is present in four scenarios out of thirteen: Ry, Rx, Rz (1 layer); Ry, Rx, Rz (5 layers); VQE: Ry, Rz, Ry + CZ (1 layer); and VQE: Ry, Rz, Ry + CZ (10 layers). After evaluating the data in Table 10, it was found that the medians were higher for scenarios involving eight features (respectively, 57.83, 57.08, 57.63, and 53.40) than for those with five features (respectively, 56.73, 55.76, 56.98, and 53.05).

Table 11 – CWRU and JNU: Mann-Whitney U test results.

Model	**Metrics**	**CWRU**	**JNU**
MLP	U	46.00	48.00
	pvalue	0.3952	0.2854
Ry, Rx, Rz (1 layer)	U	40.50	15.00
	pvalue	0.2481	**0.0046**
Ry, Rx, Rz (5 layers)	U	37.00	22.00
	pvalue	0.1723	**0.0188**
Ry, Rx, Rz (10 layers)	U	46.00	32.00
	pvalue	0.3955	0.0929
VQE: Ry, Rz, Ry + CNOT (1 layer)	U	42.00	32.00
	pvalue	0.2854	0.0929
VQE: Ry, Rz, Ry + CNOT (5 layers)	U	33.00	38.00
	pvalue	0.1061	0.1923
VQE: Ry, Rz, Ry + CNOT (10 layers)	U	39.00	29.00
	pvalue	0.2137	0.0606
VQE: Ry, Rz, Ry + CZ (1 layer)	U	36.00	24.00
	pvalue	0.1537	**0.0270**
VQE: Ry, Rz, Ry + CZ (5 layers)	U	41.50	47.00
	pvalue	0.2726	0.4251
VQE: Ry, Rz, Ry + CZ (10 layers)	U	30.00	9.00
	pvalue	0.0702	**0.0011**
VQE: Ry, Rz, Ry + *i*SWAP (1 layer)	U	40.5	29.00
	pvalue	0.2473	0.0606
VQE: Ry, Rz, Ry + *i*SWAP (5 layers)	U	32	44.00
	pvalue	0.0929	0.3388
VQE: Ry, Rz, Ry + *i*SWAP (10 layers)	U	47.00	32.00
	pvalue	0.4251	0.0929

Source: The author (2023)

For the analysis of quantum operations, merging points (2) and (3) is interesting. We can clearly identify in Table 5 that the model with the CZ entanglement gate and five layers has the greenest results in CWRU in all calculated metrics. The frameworks that followed it involved only rotations in a single layer and the CZ itself with one layer.

Zooming in on each of the models, starting with just rotation gates, one sees that with five features, the behavior of the results is decreasing. With eight features, this varies a bit, but generally, the best performances are with only one layer.

The model with CNOT is one of the worst overall; the results mostly vary from yellow to reddish, with no green points. As said before, the entanglement gate gains prominence, especially in the scenario with five layers. And its worst results are in the increase to 10 layers. Finally, *i*SWAP shows average results with some highlights, mainly with eight features.

In JNU, Table 7, the highlights in green are divided between just rotations, followed by *i*SWAP, CZ, and again, lastly, CNOT. In most cases with just rotations, the behavior when varying the layers is also mostly decreasing, i.e., the best results remain in the first layer as in CWRU. The same is true for CZ and *i*SWAP. In CNOT, however, this changes somewhat, as the negative highlights this time are in the first layer.

Thus, overall, the scenario with the rotation gates did relatively well for the two databases. CZ got the best accuracy values, but at some points, especially for JNU, it had very reddish values. It is seen that CNOT did not manage to be outstanding, and we can indicate it as the structure with entanglement presenting the worst performance for both databases.

We performed the Kruskall-Wallis statistical test for independent random samples (MONTGOMERY; RUNGER, 2010) to evaluate the hypothesis that the medians of the balanced accuracies of the models are equal. In other words, we want to assess whether the balanced accuracy scores vary based on the "model" factor. We used the same samples from Table 9 and Table 10.

For the execution of the statistical test, we set the following hypotheses: H_0 - The medians of all samples are equal; H_1: At least two medians are different. The H_{obs} test statistic follows a chi-squared distribution with degrees of freedom (d.f.) = 12 (13 -1). This is a right-tailed test (that is, we will reject the null hypothesis of equal medians if H exceeds its critical value) (MONTGOMERY; RUNGER, 2010). For d.f. = 12 we obtain the critical value (21.0261) for a significance level equal to 0.05.

We conducted the test for four different scenarios: CWRU and JNU with 5 and 8 features. In Table 12, we can observe the test statistics and the obtained p-values. In all cases, the null hypotheses were rejected since the statistics exceed the critical value. Thus, we can

infer that, statistically, at least two medians among the models differ and the balanced accuracy scores vary based on the model factor. The presented highlights of results support the notion that certain models consistently demonstrate suboptimal performance, particularly those utilizing CNOT. On the other hand, some models, such as the VQE with CZ, exhibit superior results.

Table 12– CWRU and JNU: Kruskal-Wallis test results.

Metrics	**CWRU**		**JNU**	
	5 features	**8 features**	**5 features**	**8 features**
H_{obs}	42.6283	47.9495	86.7778	93.2312
pvalue	2.61e − 05	3.19e − 06	2.0698e-13	1.1659e-14

Source: The author (2023).

When using the quantum simulator, there was no pattern regarding the increase in the number of layers and the improvement of the metrics. The results were generally better with up to five layers, decreasing when composing the circuit with ten layers. But there were cases where the inverse also happened.

Therefore, based on all findings, some QML models outperformed MLP in the calculated metrics. However, many other ML model configurations could be compared. In this study, it is not possible to judge whether the higher complexity DL algorithms are better than those of QML. Some studies in the literature apply DL methods that can achieve 100% accuracy, as in Zhao *et al*. (2020), as we observed in sections 4.1.1 and 4.2.1, but differently from our case, they use the full signal and have no input size limitations. We emphasize that the main focus is to show the applicability of these QML methods – on the rise in the literature (BIAMONTE *et al*., 2017; BROUGHTON *et al*., 2020; PERDOMO-ORTIZ *et al*., 2018) – in Reliability Engineering and to encourage their exploration in different machinery, sectors, and contexts that demand PHM activities, which are valuable to support maintenance decisions.

Finally, Table 13 shows the computational times, measured in seconds, required to train the models for the two databases (CWRU and JNU). The first point is that the classical MLP model achieves significantly less training time than the QML ones. The reason for this is that the models were trained on a simulator. Actual quantum hardware would likely achieve more agile times than those presented here.

Table 13 - CWRU and JNU run times run times in seconds by model.

Category	Quantum gates	# of circuit layers	Run time (seconds)			
			CWRU		JNU	
			5 features	8 features	5 features	8 features
Classic ML (MLP)	-	-	3.00	1.30	7.30	7.41
QML	**Ry, Rx, Rz**	1	18.73	40.39	579.99	394.82
		5	36.30	74.44	751.31	1062.08
		10	86.31	168.38	875.50	3011.48
	VQE: Ry, Rz, Ry + CNOT	1	27.50	65.36	162.99	506.52
		5	51.11	128.81	1211.89	684.67
		10	75.43	220.98	2020.91	2583.07
	VQE: Ry, Rz, Ry + CNOT	1	28.69	41.19	261.53	591.85
		5	70.47	173.35	555.65	2253.73
		10	121.43	505.76	1714.18	3612.71
	VQE: Ry, Rz, Ry + CNOT	1	25.18	45.34	361.11	538.44
		5	68.56	90.58	1117.64	1378.35
		10	147.63	353.91	2526.39	2377.20

Source: The author (2023).

When comparing the quantum models with each other, the fewer layers in the circuit, the faster the training becomes since the number of operations is smaller. It occurs in all scenarios.

The training time of JNU is significantly longer than that of CWRU due to the complexity of the former. Lastly, we note that due to the early stopping inserted in training, some processes have more epochs than others, as presented in Figure 15. Consequently, some training takes longer than others as well. Also, models with eight features, in most cases, have longer processing times than those with five features. That is, possibly the increase in the number of qubits also influences the longer processing time.

5 CONCLUDING REMARKS

5.1 CONCLUSIONS

The main objective of this work was to use QML for the PHM of of equipment that can be used in the O&G industry. We bring results regarding bearing data available in the literature. These components compose different and important equipment in the O&G industry as shown in Orrù *et al* (2020) study. The framework of the QML models was based on an existing approach, but they have different combinations in the quantum part itself. That is, the PQCs have other configurations besides the rotations gates. These are: the increment of the VQE algorithm combined with different two-qubit gates (CNOT, CZ and iSWAP). Still additional layers of these circuits were added to identify if the increment of quantum operations, such as entanglement, would bring differences in the results.

Using just signals in the time domain, regarding the CWRU, the model with CZ and 5 layers presented higher accuracy of the training data in relation to the others. Therefore, the effectiveness of a hybrid-quantum model for the diagnosis of failure modes for this type of equipment can be attested to in the scope of this study. As partial results, it was seen that when compared to the MLP model that has the same neural network configuration used for the quantum models, the QML results were better overall.

Concerning JNU, the best model in terms of accuracy was the VQE with CZ entanglement gates with 1 circuit layer. In this database, the model with the lowest accuracy was the MLP in both features configuration (5 and 8).

When comparing with benchmarks available in the literature (ZHAO *et al.*, 2020), it was seen that the QML models studied in this paper overlap MLP and AE only in the time domain. In the frequency domain the classical models still have better results. Thus, it opens the possibility for new QML models to be explored, since there are many and diverse ways to build such systems, which can excel what is already known classically in academia.

The contributions of this work are outlined in the following aspects: (1) exploration of two databases in the literature not yet analyzed in the QML framework; (2) performance of the diagnosis of a larger number of failure modes, compared to what has already been done in the literature; (3) delineation of the limitations of this study that can be a start kick for improvements and execution of new studies that cover the gaps of this one, as will be described throughout this conclusion; and, (4) to conduct a proof of concept that new quantum computing technologies can be used in Reliability Engineering problems, specifically in the diagnosis of

failure modes of rotating machinery components, which are widely used in the O&G industry. Interested organizations may also be able to follow QC trends to modernize actions to help develop maintenance policies that are key points for the success of productive operations and safety.

The outcomes supported the notion that the proposed QML models constitute a promising strategy for handling features extractions of times series from multi-sensor suites for complex systems' health state diagnosis. It must be emphasized that, so far, there are many limitations in terms of computational capacity of quantum programs, as will be mentioned in the next session. However, this is a promising path that tends to gain popularity in academia and companies. Quantum Computing has been receiving growing investments in terms of hardware in order to enable the resolution of problems with larger instances in a more efficient way.

5.2 LIMITATIONS AND FUTURE WORKS

Despite the promising results, the QML models, given the framework we are using, is limited to the maximum number of qubits that the quantum library simulator, from TensorFlow Quantum, makes available. Thus, it is not possible to use the complete series, reducing the analysis only to features. It is possible that some data information is lost during the analysis. Also, we peformed our models using just the TensorFlow Quantum simulator. In this sense, the execution time in this type of software is much longer than when using a quantum machine. Thus, for future work it is suggested to use a QC hardware to improve performance in this regard and observe some quantum variables as noises.

Another limitation refers to the number of layers used in the circuit. Due to the computational capacity, it was not possible to apply more than 10 layers. In this case, it is assumed that the greater the number of layers, the greater the effect of quantum properties, such as entanglement. However, this study is limited only to the observations presented here. Nevertheless, it is suggested for future studies the application of other configurations of quantum circuits, such as the QAOA architecture. Finally, exploring different backpropagation methods in addition to the finite difference technique used in this work, such as the parameter-shift rule, could bring valuable insights.

In the preprocessing scheme, the inputs where preprocessing only in the time and in the frequency domain. However, there are other configurations that may be explored tofit the models, for example, the Short Time Fourier Transform (STFT) and the Continuous Wavelet

Transform (CWT). Also, as the main purpose of this work was to vary the PQC of the model, the classical neural network used remained the same in every scenario. In this sense, to future works it is suggested that other NN schemes be tested for network efficiency observation.

The code library is available at:
https://github.com/laviniammaraujo/MasterThesis_PHMviaQML.

REFERENCES

ANTONI, J.; BORGHESANI, P. A statistical methodology for the design of condition indicators. **Mechanical Systems and Signal Processing**, v. 114, p. 290–327, 2019.

ARAÚJO, L. M. M. *et al*. Technology Selection and Risk Assessment through Equipment Development in Oil & Gas Industry: A Literature Review. **5th Abrisco.** 2021.

ARAÚJO, L. M. M. *et al*. Hyperparameter Optimization of Bayesian Prior Distribution Through Equipment Development in O&G Industry: a Literature Review. **LIV Simpósio Brasileiro de Pesquisa Operacional**. 2022a.

ARAÚJO, L. M. M. *et al*. Review of Quantum (-Inspired) Optimization Methods for System Reliability Problems. **Probabilistic Safety Assessment and Management PSAM 16**. 2022b.

ARAÚJO, L. M. M. *et al*. A Quantum Optimization Modeling for Redundancy Allocation Problems. 32nd European Safety and Reliability Conference. **32nd European Safety and Reliability Conference**, 2022c.

BARRAZA, J. F. *et al*. Deep learning health state prognostics of physical assets in the Oil and Gas industry. Proceedings of the Institution of Mechanical Engineers, Part O: **Journal of Risk and Reliability**, v. 236, n. 4, p. 598–616, 2022.

BEYER, J. *et al*. Environmental effects of the Deepwater Horizon oil spill: A review. **MPB**, v. 110, n. 1, p. 28–51, 2016.

BIAMONTE, J. *et al*. Quantum machine learning. **Nature**, v. 549, n. 7671, p. 195–202, 2017.

BROUGHTON, M. *et al*. TensorFlow Quantum: A Software Framework for Quantum Machine Learning. **arXiv preprint arXiv:2003.02989**, 2020.

CHANDRASEGARAN, D.; GHAZILLA, R. A. R.; RICH, Karl. Human factors engineering integration in the offshore O&G industry: A review of current state of practice. **Safety science**, v. 125, p. 104627, 2020.

CHIANG, H. P. *et al*. A quantum-inspired Tabu search algorithm for solving combinatorial optimization problems. **Soft Computing**, v. 18, n. 9, p. 1771–1781, 2014.

CORREA-JULLIAN, C. *et al*. Exploring Quantum Machine Learning and Feature Reduction Techniques for Wind Turbine Pitch Fault Detection. **Energies**, v. 15, n. 8, p. 1–29, 2022.

CWRU. **Case Western Reserve University Bearing Data Center Website**. 2020. Available at: <https://csegroups.case.edu/bearingdatacenter/pages/welcome-case-western-reserve-university-bearing-data-center-website>. Accessed on: June 10th, 2022.

GARCÍA, D. P.; CRUZ-BENITO, J.; GARCÍA-PEÑALVO, F. J. Systematic Literature Review: Quantum Machine Learning and its applications. **arXiv preprint arXiv:2201.04093**, 2022.

GIL, A. C, *et al*. **Como elaborar projetos de pesquisa**. São Paulo: Atlas, 2002.

HABES, M. *et al*. The role of modern media technology in improving collaborative learning of students in Jordanian universities. **Int. J. Inf. Technol. Lang. Stud.** v. 2, p. 71–82, 2018.

HARROW, A. W.; MONTANARO, A. Quantum computational supremacy. **Nature**, v. 549, n. 7671, p. 203–209, set. 2017.

HEMMATI, F.; ORFALI, W.; GADALA, M. S. Roller bearing acoustic signature extraction by wavelet packet transform, applications in fault detection and size estimation. **Applied Acoustic**s, v. 104, p. 101–118, 2016.

ISLAM, M. M. M.; KIM, J. M. Automated bearing fault diagnosis scheme using 2D representation of wavelet packet transform and deep convolutional neural network. **Computers in Industry**, v. 106, p. 142–153, 2019.

JAVED, K.; GOURIVEAU, R.; ZERHOUNI, N. State of the art and taxonomy of prognostics approaches, trends of prognostics applications and open issues towards maturity at different technology readiness levels. **Mechanical Systems and Signal Processing**, v. 94, p. 214–236, 2017.

JNU. **JNU dataset**. 2019 Available at: <http://mad-net.org:8765/explore.html?t=0.5831516555847212>. Accessed on: June 10th, 2022.

KAVITHA, S. S.; KAULGUD, N. Quantum machine learning for support vector machine classification. **Evolutionary Intelligence**, p. 1-10, 2022.

KHALAF, A. M.; SEIBI, A. C. Failure analysis of lube oil feed tube of a gas turbine operating in oil fields. **Engineering Failure Analysis**, v. 18, n. 5, p. 1341–1350, 2011.

KHAN, T. M.; ROBLES-KELLY, A. Machine Learning: Quantum vs Classical. **IEEE**

Access, v. 8, p. 219275–219294, 2020.

KIM, Y. *et al*. Phase-based time domain averaging (PTDA) for fault detection of a gearbox in an industrial robot using vibration signals. **Mechanical systems and signal processing.** v. 138, n. 2020, p. 106544, 2021.

KONAR, D. *et al*. An improved Hybrid Quantum-Inspired Genetic Algorithm (HQIGA) for scheduling of real-time task in multiprocessor system. **Applied Soft Computing Journal**, v. 53, p. 296–307, 2017.

KUMAR, A.; SHANKAR, R.; THAKUR, L. S. A big data driven sustainable manufacturing framework for condition-based maintenance prediction. **Journal of Computational Science,** v. 27, p. 428–439, 2018.

LI, K. *et al*. Sequential fuzzy diagnosis method for motor roller bearing in variable operating conditions based on vibration analysis. **Sensors (Switzerland**), v. 13, n. 6, p. 8013–8041, 2013.

LI, Y. *et al*. An enhanced morphology gradient product filter for bearing fault detection. **Mechanical Systems and Signal Processing**, v. 109, p. 166–184, 2018.

LINS, I. D. *et al*. Computing confidence and prediction intervals of industrial equipment degradation by bootstrapped support vector regression. **Reliability Engineering and System Safety**, v. 137, p. 120–128, 2015.

LIU, Y. *et al*. A conditional variational autoencoding generative adversarial networks with self-modulation for rolling bearing fault diagnosis. **Measurement: Journal of the International Measurement Confederation**, v. 192, n. September 2021, p. 110888, 2022.

LUCAS, T. *et al*. Diagnosis of Failure Modes from Bearing Data via Deep Learning Variational Autoencoder Method. **Probabilistic Safety Assessment and Management PSAM 16**. 2022.

LYBECK, N.; MARBLE, S.; MORTON, B. Validating prognostic algorithms: A case study using comprehensive bearing fault data. **IEEE Aerospace Conference Proceedings**, 2007.

MAIOR, C. B. S. *et al*. Bayesian prior distribution based on generic data and experts' opinion: a case study in the O&G industry. **Journal of Petroleum Science and Engineering**, v. 210, n. 0920–4105, 2022.

MAIOR, C. B. S.; MOURA, M. C.; LINS, I. D. Particle swarm-optimized support vector machines and pre-processing techniques for remaining useful life estimation of bearings.

Eksploatacja i Niezawodnosc - Maintenance and reliability, v. 21, n. 4, p. 610–619, 2019.

MONTANARO, A. Quantum algorithms: An overview. npj **Quantum Information**, v. 2, n. 1, p. 1–8, 2016.

MONTGOMERY, D. C.; RUNGER, G. C. **Applied Statistics and Probability for Engineers**. John wiley & sons, Fifth Ed. 2010.

NAWAZ, S. J. *et al*. Quantum Machine Learning for 6G Communication Networks: State-of-the-Art and Vision for the Future. **IEEE Access**, v. 7, p. 46317–46350, 2019.

NAYANA, B. R.; GEETHANJALI, P. Analysis of Statistical Time-Domain Features Effectiveness in Identification of Bearing Faults From Vibration Signal. **IEEE Sensors Journal.** v. 17, n. 17, p. 5618–5625, 2017.

NIELSEN, M. A.; CHUANG, I.. **Quantum computation and quantum information.** 2010.

OLECHOWSKI, A. L.; EPPINGER, S. D.; JOGLEKAR, N. Technology Readiness Levels at 40: A Study of State-of-the-Art Use, Challenges, and Opportunities. **SSRN Electronic Journal**, p. 0–28, 2015.

ORHAN, S.; AKTÜRK, N.; ÇELIK, V. Vibration monitoring for defect diagnosis of rolling element bearings as a predictive maintenance tool: Comprehensive case studies. **NDT and E International**, v. 39, n. 4, p. 293–298, 2006.

ORRÙ, P. F. *et al*. Machine learning approach using MLP and SVM algorithms for the fault prediction of a centrifugal pump in the oil and gas industry. **Sustainability (Switzerland**), v. 12, n. 11, 2020.

OSABA, E. *et al*. Hybrid Quantum Computing - Tabu Search Algorithm for Partitioning Problems: Preliminary Study on the Traveling Salesman Problem. **IEEE Congress on Evolutionary Computation**, CEC 2021 - Proceedings, p. 351–358, 2021.

PANETTA, P. D.; POTTER, S. TRL definitions for oil spill response technologies and equipment. **Applied Research Associates, The College of William & Mary, Virginia Institute of Marine Science, and SL Ross.(Bureau of Safety and Environmental Enforcement Project 1042)**, 2016.

PERDOMO-ORTIZ, Alejandro *et al*. Opportunities and challenges for quantum-assisted machine learning in near-term quantum computers. **Quantum Science and Technology**, v. 3, n. 3, p. 030502, 2018.

PERRONS, R. K. How innovation and R & D happen in the upstream oil & gas industry : Insights from a global survey. **Journal of Petroleum Science and Engineering**, v. 124, p. 301–312, 2014.

PERUCHI, R. S. *et al*. Integrating Multivariate Statistical Analysis into Six Sigma DMAIC Projects: A Case Study on AISI 52100 Hardened Steel Turning. **IEEE Access**, v. 8, p. 34246–34255, 2020.

PRAKASH, K. B.. Quantum Meta-Heuristics and Applications. Cognitive Engineering for Next Generation Computing: **A Practical Analytical Approach**, p. 265-297, 2021.

QUATRINI, E. *et al*. Condition-Based Maintenance — An Extensive Literature Review. **Machines**, v. 8, n. 2, p. 31, 2020.

RASMUSSEN, S. E.; ZINNER, N. T. Parameterized Two-Qubit Gates for Enhanced Variational Quantum Eigensolver. **Annalen der Physik**, p. 2200338, 2022.

RIEFFEL, Eleanor G.; POLAK, Wolfgang H. Quantum computing: A gentle introduction. **MIT Press**, 2011.

ROSER, B. *et al*. Bias, precision, and accuracy of skewness and kurtosis estimators for frequently used continuous distributions. **Symmetry**, v. 12, n. 19, p. 2–17, 2020.

ROYCHOUDHURY, I. *et al*. Distilling the verification process for prognostics algorithms. **PHM 2013 - Proceedings of the Annual Conference of the Prognostics and Health Management Society 2013**, p. 220–229, 2013.

SAIMURUGAN, M. *et al*. Multi component fault diagnosis of rotational mechanical system based on decision tree and support vector machine. **Expert Systems with Applications**, v. 38, n. 4, p. 3819–3826, 2011.

SARAYGORD AFSHARI, S. *et al*. Machine learning-based methods in structural reliability analysis: A review**. Reliability Engineering and System Safety**, v. 219, n. August 2021, p. 108223, 2022.

SCHOLTEN, K.; DE BLOK, C.; HAAR, R.. How flexibility accommodates demand variability in a service chain: insights from exploratory interviews in the refugee supply chain. In: **The Palgrave Handbook of Humanitarian Logistics and Supply Chain Management. Palgrave Macmillan**, London, 2018. p. 359-393.

SHAFIEE, M.; ELUSAKIN, T.; ENJEMA, E. Subsea blowout preventer (BOP): Design,

reliability, testing, deployment, and operation and maintenance challenges. **Journal of Loss Prevention in the Process Industries**, v. 66, n. July 2019, p. 104170, 2020.

SHAREEF, H. *et al*. Electrical Power and Energy Systems Power quality and reliability enhancement in distribution systems via optimum network reconfiguration by using quantum firefly algorithm. **INTERNATIONAL JOURNAL OF ELECTRICAL POWER AND ENERGY SYSTEMS**, v. 58, p. 160–169, 2014.

SHARMA, S. K.; CHANDA, U. Developing a Bayesian belief network model for prediction of R&D project success. Journal of Management Analytics, v. 4, n. 3, p. 321–344, 2017.

SIERRA-SOSA, D.; TELAHUN, M.; ELMAGHRABY, A. TensorFlow Quantum: Impacts of Quantum State Preparation on Quantum Machine Learning Performance. **IEEE Access**, v. 8, p. 215246–215255, 2020.

SILVA, G. S. M.; DROGUETT, E. L. Quantum Machine Learning for Health State Diagnosis and Prognostics. In: **2022 Annual Reliability and Maintainability Symposium (RAMS)**. IEEE, 2022. p. 1-7.

SONG, L.; WANG, H.; CHEN, P. Vibration-Based Intelligent Fault Diagnosis for Roller Bearings in Low-Speed Rotating Machinery. **IEEE Transactions on Instrumentation and Measurement**, v. 67, n. 8, p. 1887–1899, 2018.

TAMALA, J. K. *et al*. A bibliometric analysis of sustainable oil and gas production research using VOSviewer. **Cleaner Engineering and Technology,** v. 7, p. 100437, 2022.

TILLY, J. *et al*. The Variational Quantum Eigensolver: A review of methods and best practices. **Physics Reports,** v. 986, p. 1–128, 2022.

TOMASCHEK, K. *et al*. A Survey of Technology Readiness Level Users. **INCOSE International Symposium**, v. 26, n. 1, p. 2101–2117, 2016.

WANG, S. *et al*. Matching Synchrosqueezing Wavelet Transform and Application to Aeroengine Vibration Monitoring. **IEEE Transactions on Instrumentation and Measurement**, v. 66, n. 2, p. 360–372, 2017.

WANG, Y.; LIU, H. Quantum Computing in a Statistical Context. **Annual Review of Statistics and Its Application**, v. 9, p. 479–504, 2022.

YARKONI, S. *et al*. Quantum Annealing for Industry Applications: Introduction and Review. **Reports on Progress in Physics**, v. 1, n. 1, 2021.

YE, J. *et al*. Comparison of technology qualification approaches. **Proceedings of the Annual Offshore Technology Conference**, v. 5, p. 3763–3773, 2017.

YE, Z.; YU, J. Deep morphological convolutional network for feature learning of vibration signals and its applications to gearbox fault diagnosis. **Mechanical Systems and Signal Processing**, v. 161, p. 107984, 2021.

ZHANG, S. *et al*. Semi-Supervised Bearing Fault Diagnosis and Classification Using Variational Autoencoder-Based Deep Generative Models. **IEEE Sensors Journal**, v. 21, n. 5, p. 6476–6486, 2021.

ZHANG, Y.; YANG, K. Fault Diagnosis of Submersible Motor on Offshore Platform Based on Multi-Signal Fusion. **Energies**, v. 15, n. 3, 2022.

ZHAO, D. *et al*. Enhanced data-driven fault diagnosis for machines with small and unbalanced data based on variational auto-encoder. **Measurement Science and Technology**, v. 31, n. 3, 2019.

ZHAO, Z. *et al*. Deep learning algorithms for rotating machinery intelligent diagnosis: An open source benchmark study. **ISA Transactions**, v. 107, p. 224–255, 2020.

ZONTA, T. *et al*. Predictive maintenance in the Industry 4.0: A systematic literature review. **Computers and Industrial Engineering,** v. 150, n. April 2019, p. 106889, 2020.

APPENDIX A – CWRU DATASET: CONFUSION MATRIX AND MODEL ACCURACY GRAPH WITH FIVE AND EIGHT FEATURES

Model	5 features		8 features	
	CM	Accuracy	CM	Accuracy
Ry, Rx, Rz (1 layer)	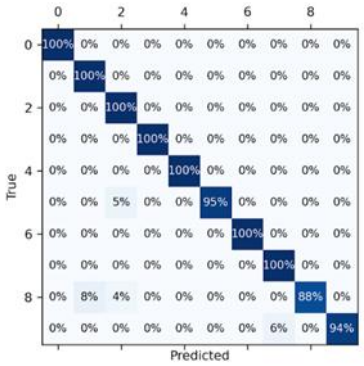	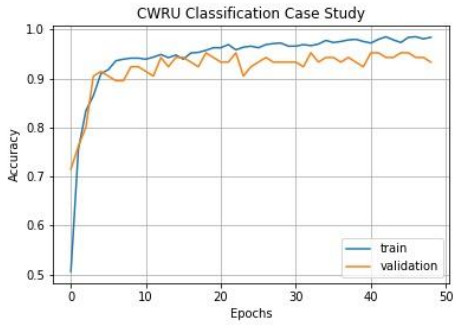	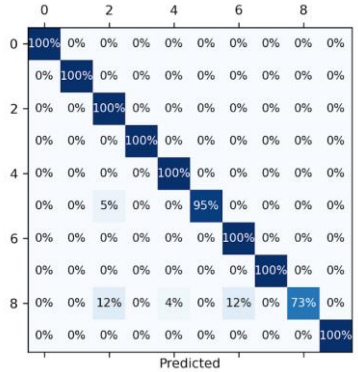	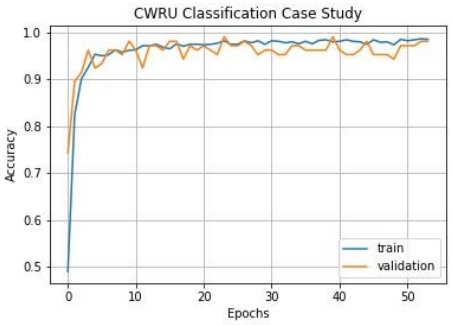
Ry, Rx, Rz (5 layers)	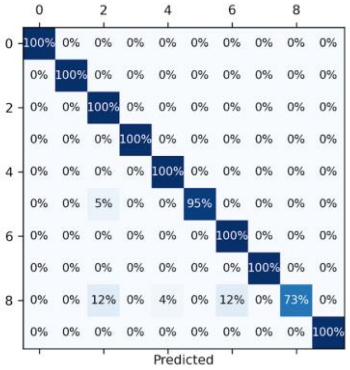	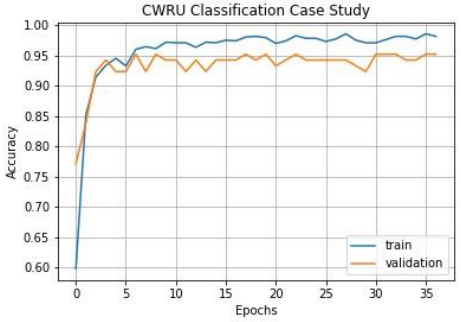	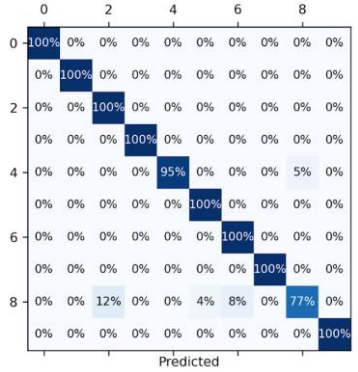	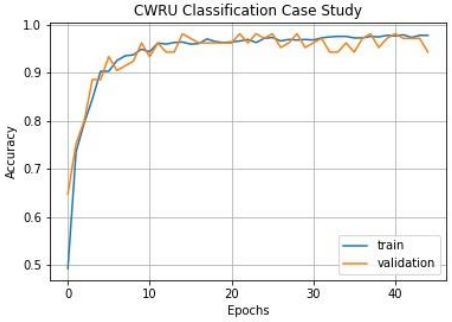

Ry, Rx, Rz (10 layers)

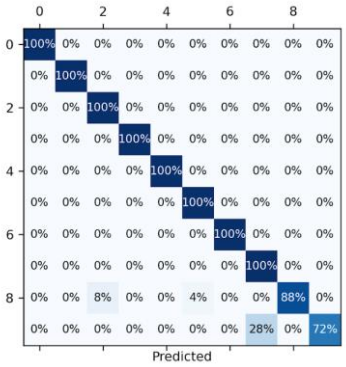

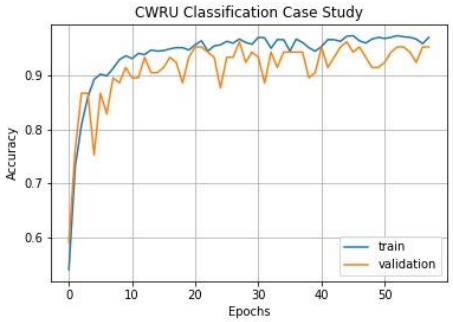

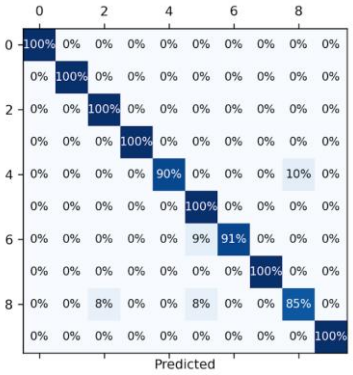

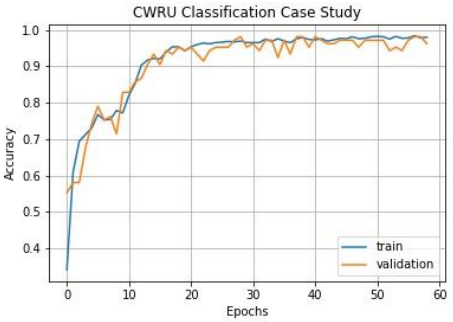

VQE: Ry, Rz, Ry + CNOT (1 layer)

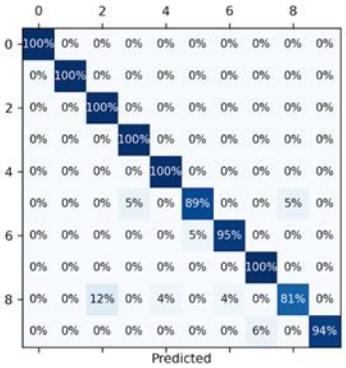

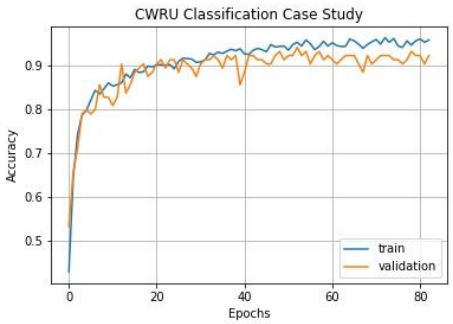

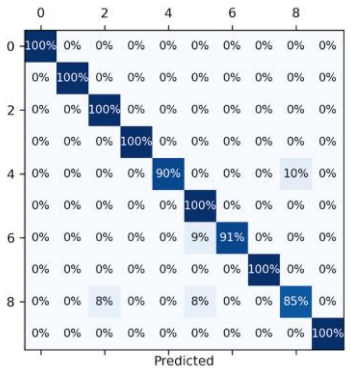

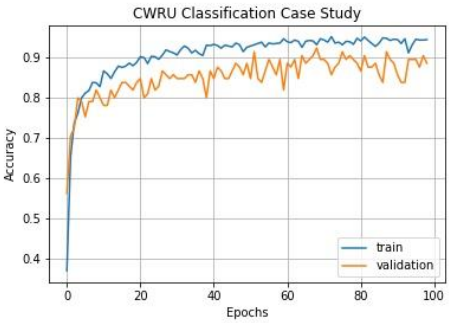

VQE: Ry, Rz, Ry + CNOT (5 layers)

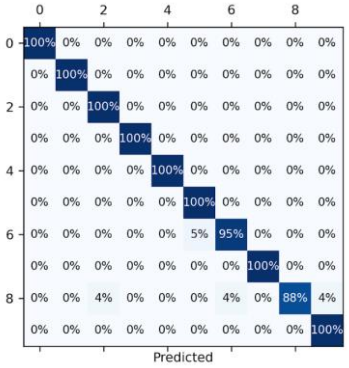

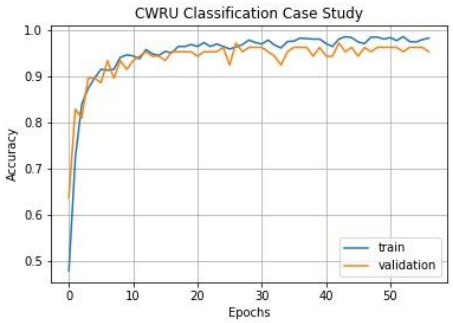

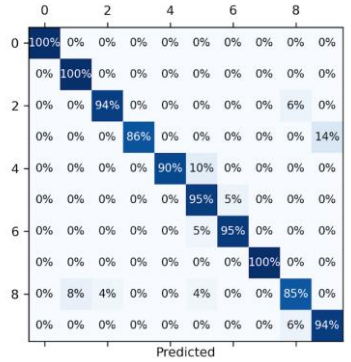

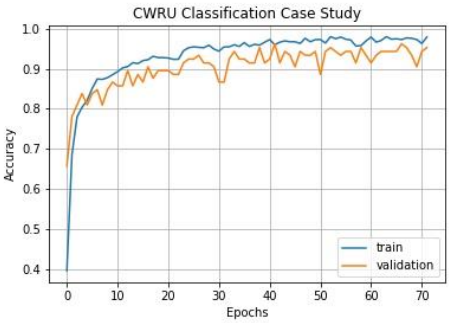

VQE: Ry, Rz, Ry + CNOT (10 layers)

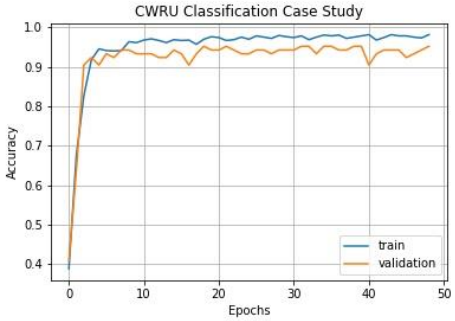

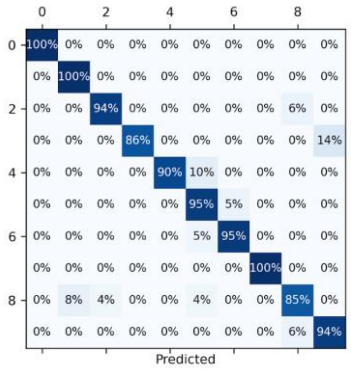

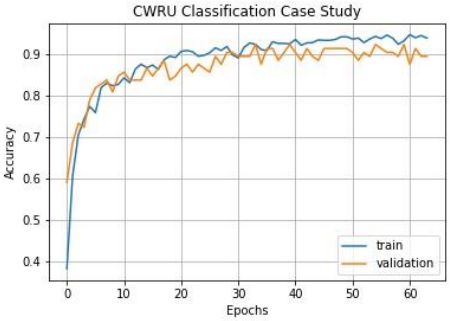

VQE: Ry, Rz, Ry + CZ (1 layer)

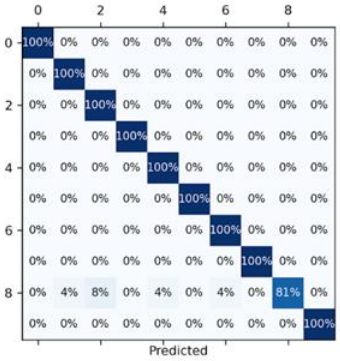

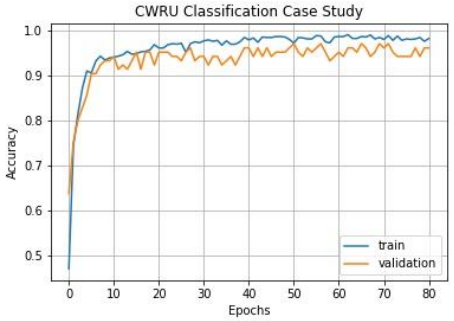

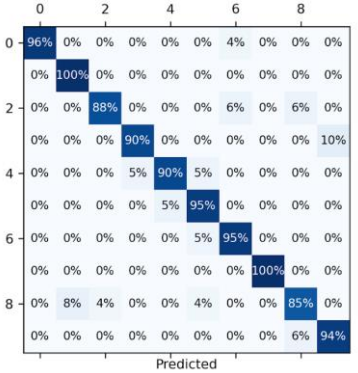

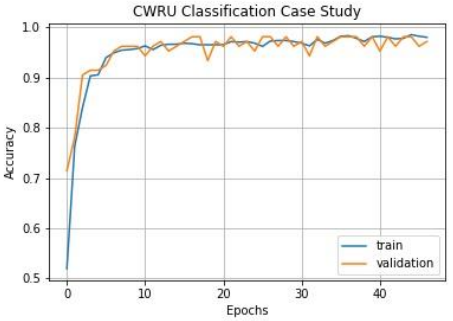

VQE: Ry, Rz, Ry + CZ (5 layers)

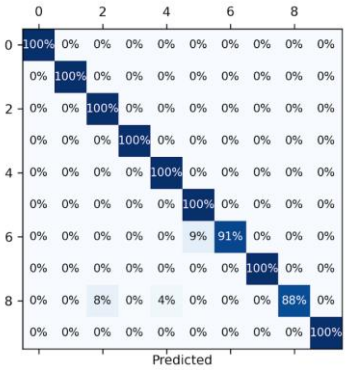

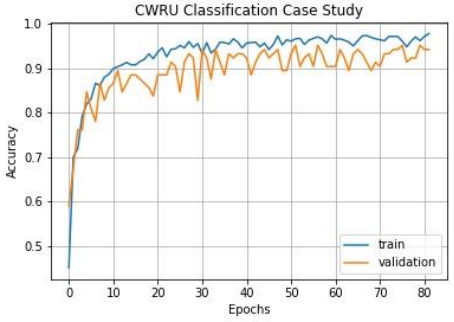

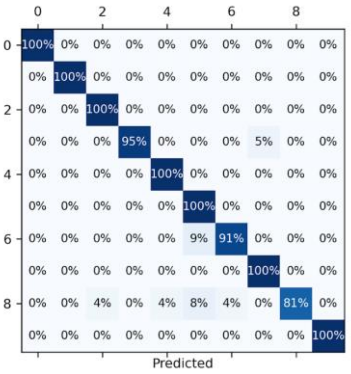

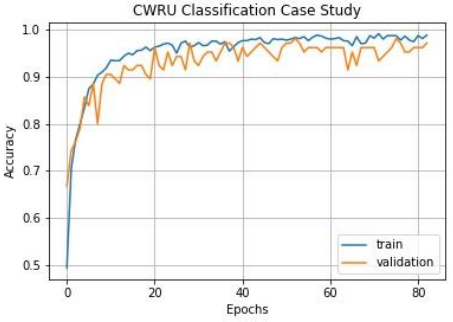

VQE: Ry, Rz, Ry + CZ (10 layers)

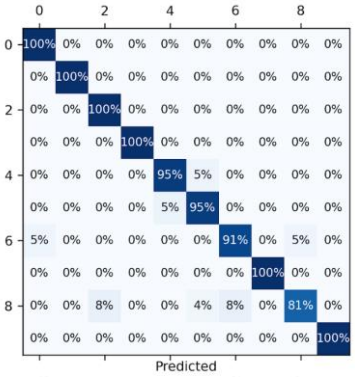

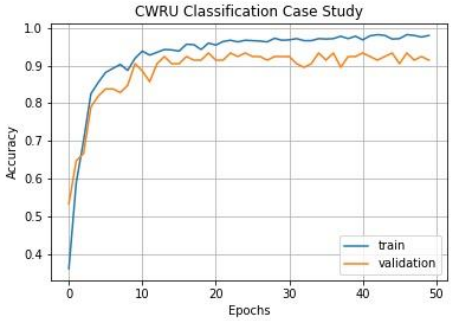

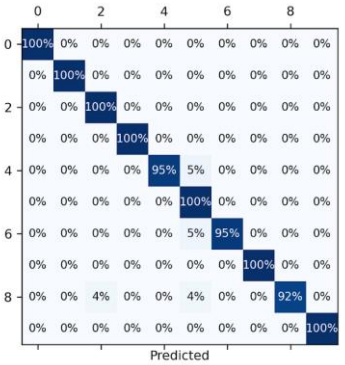

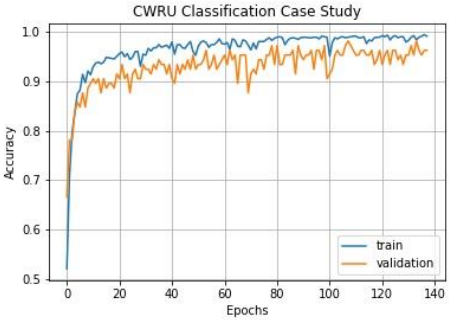

VQE: Ry, Rz, Ry + *i*SWAP (1 layer)

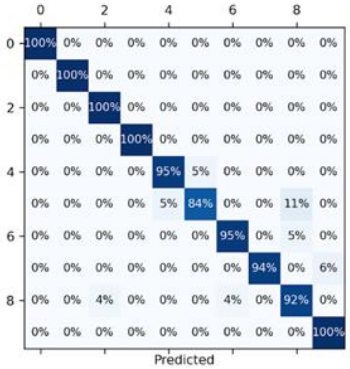

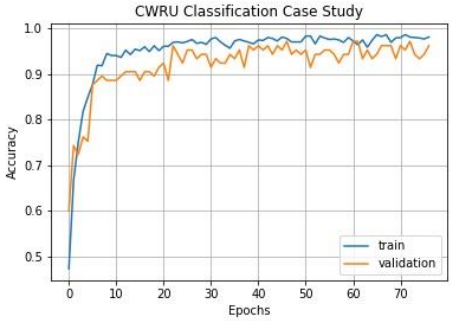

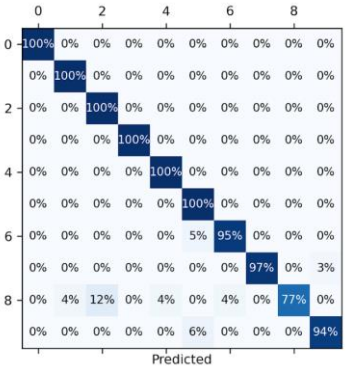

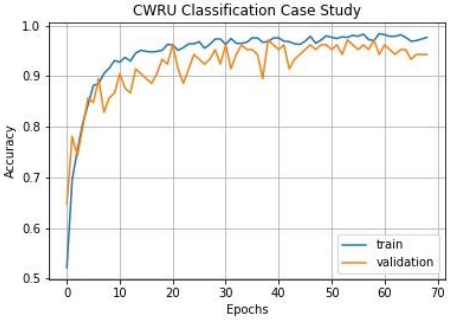

VQE: Ry, Rz, Ry + *i*SWAP (5 layers)

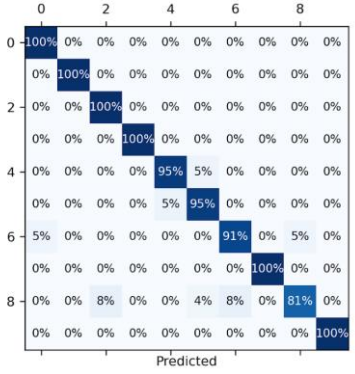

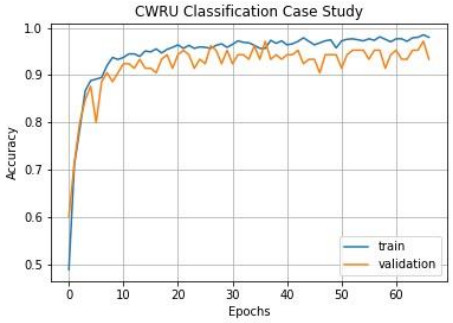

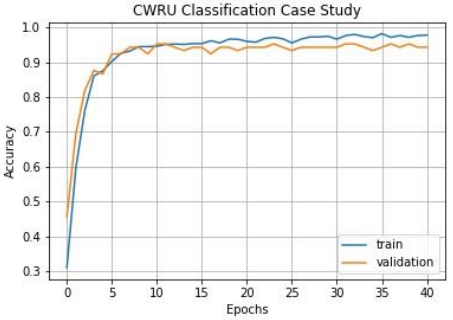

VQE: Ry, Rz, Ry + *i*SWAP (10 layers)

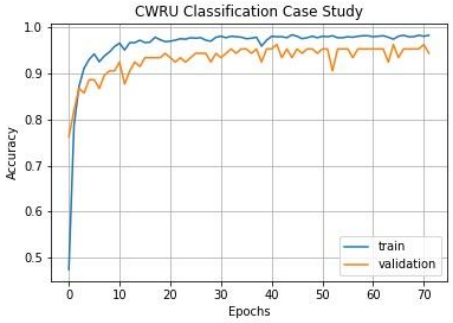

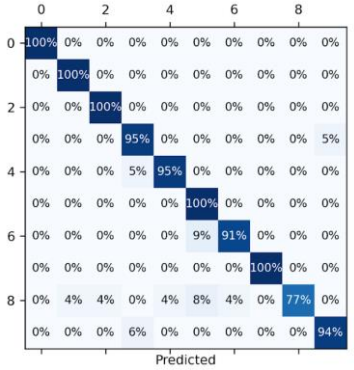

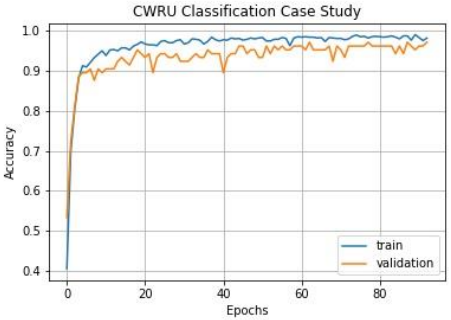

APPENDIX B – JNU DATASET: CONFUSION MATRIX AND MODEL ACCURACY GRAPH WITH FIVE AND EIGHT FEATURES

Model	5 features		8 features	
	CM	Accuracy	CM	Accuracy
Ry, Rx, Rz (1 layer)	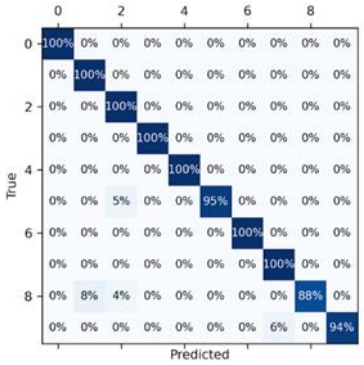	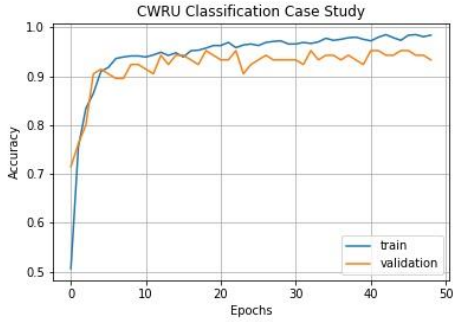	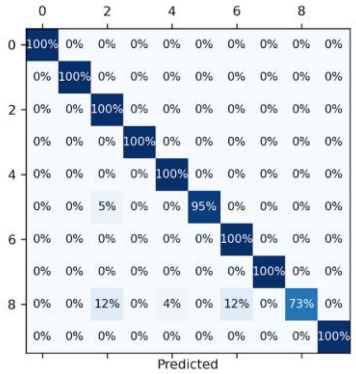	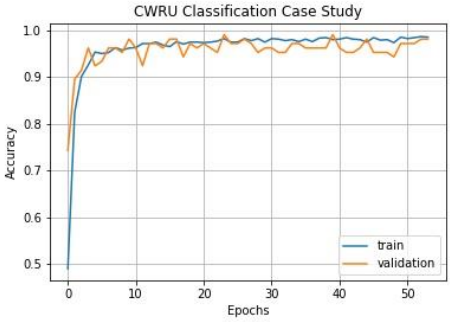
Ry, Rx, Rz (5 layers)	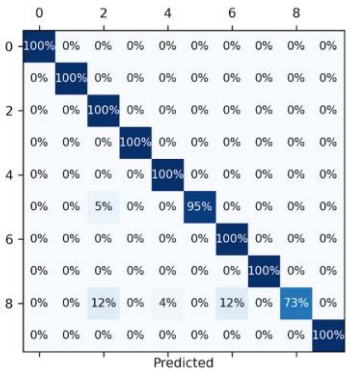	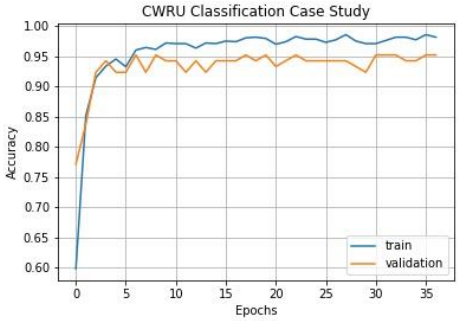	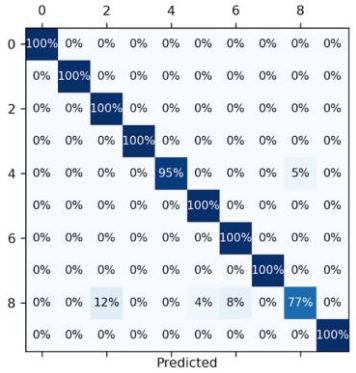	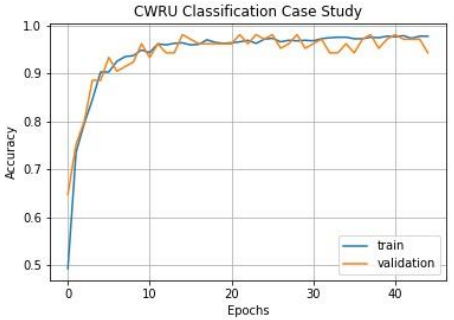

Ry, Rx, Rz (10 layers)

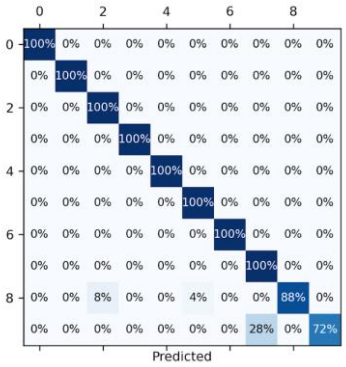

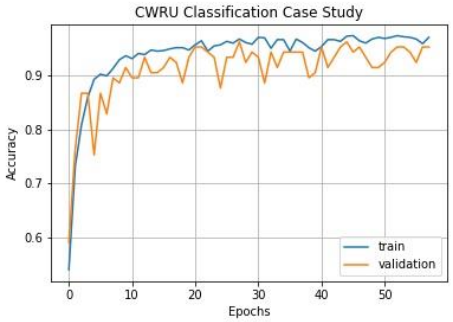

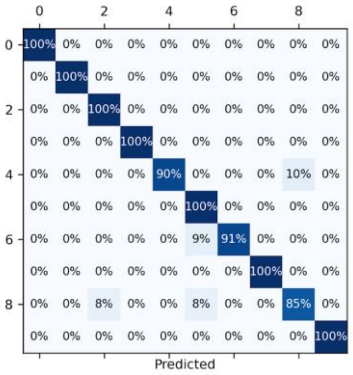

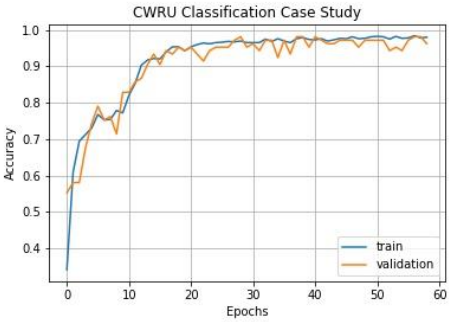

VQE: Ry, Rz, Ry + CNOT (1 layer)

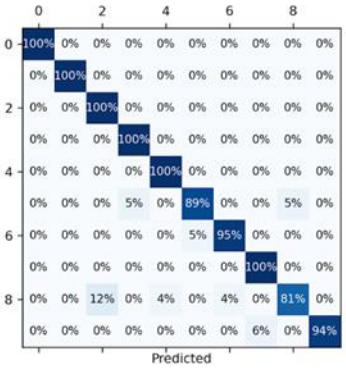

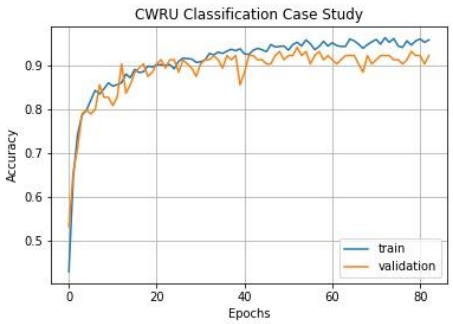

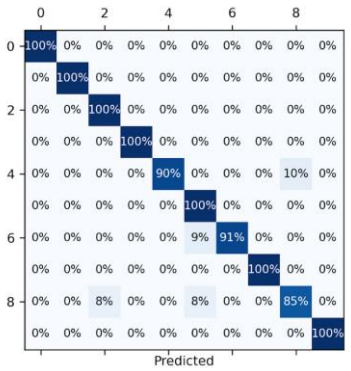

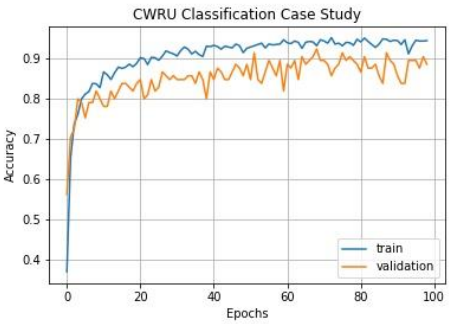

VQE: Ry, Rz, Ry + CNOT (5 layers)

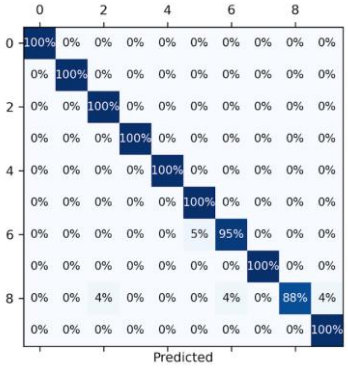

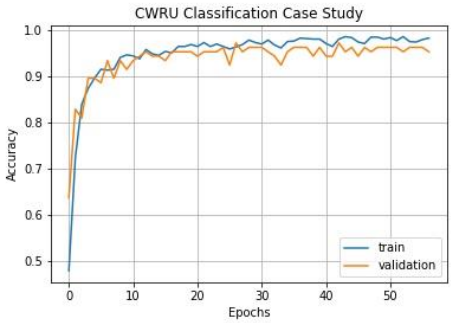

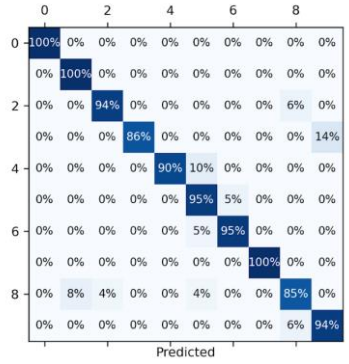

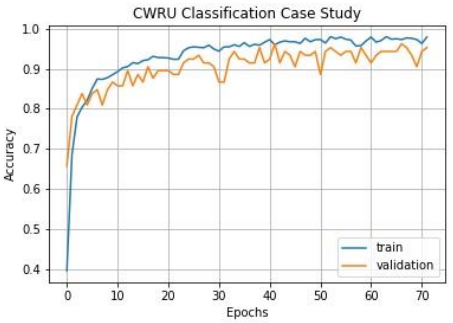

VQE: Ry, Rz, Ry + CNOT (10 layers)

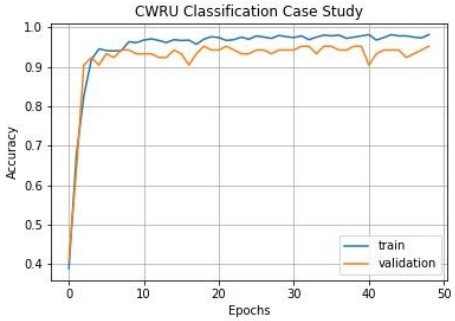

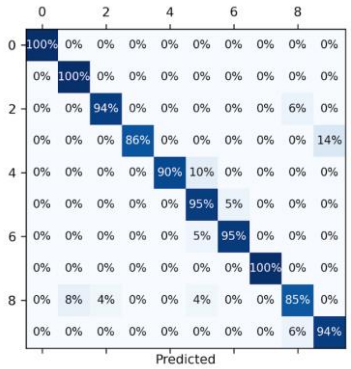

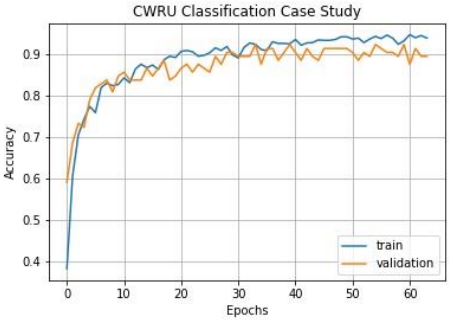

VQE: Ry, Rz, Ry + CZ (1 layer)

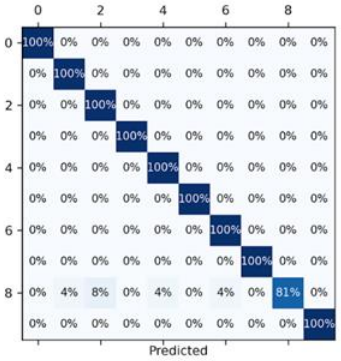

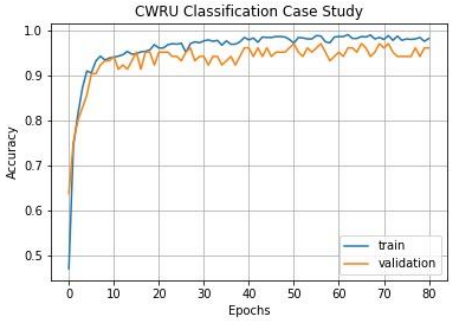

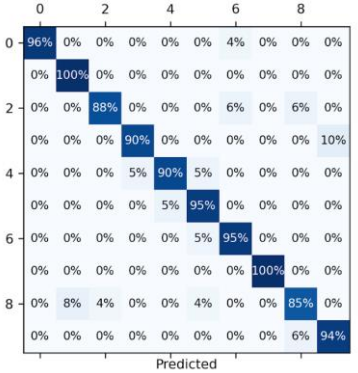

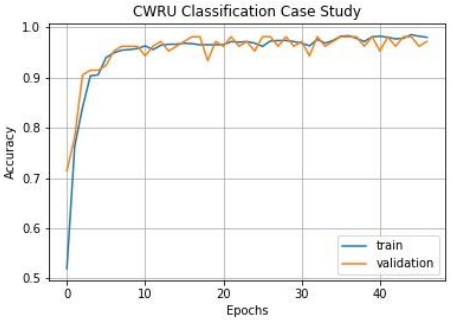

VQE: Ry, Rz, Ry + CZ (5 layers)

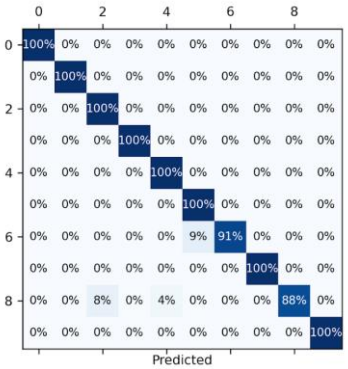

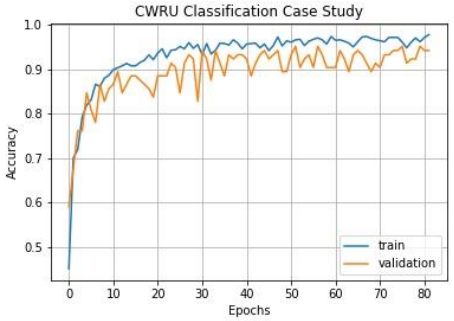

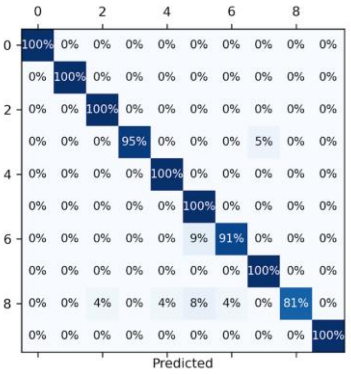

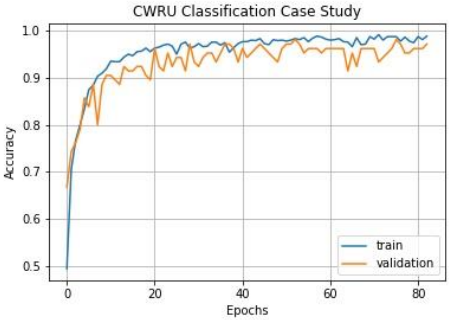

VQE: Ry, Rz, Ry + CZ (10 layers)

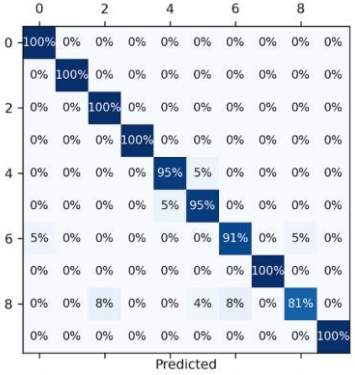

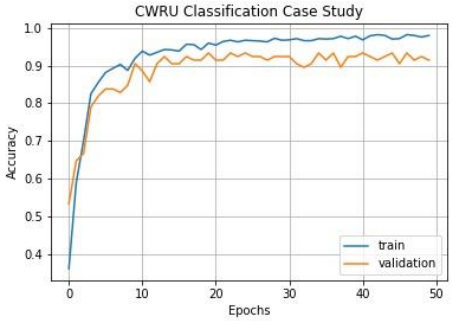

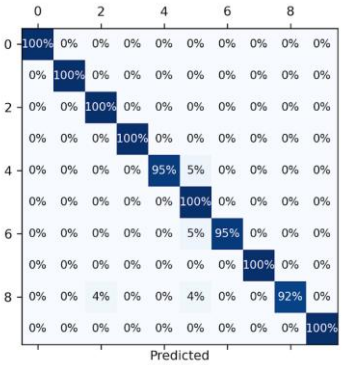

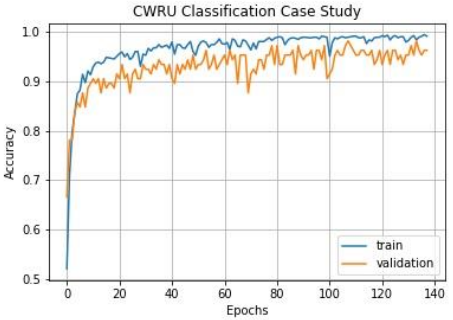

VQE: Ry, Rz, Ry + *i*SWAP (1 layer)

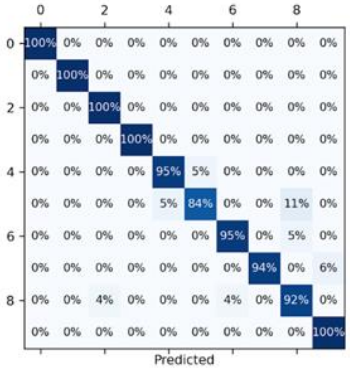

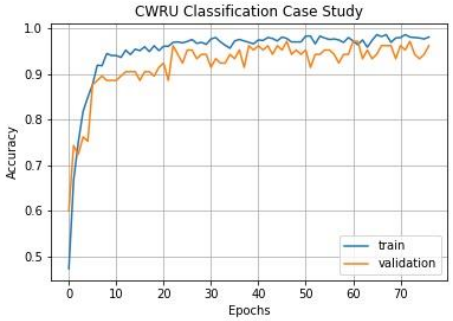

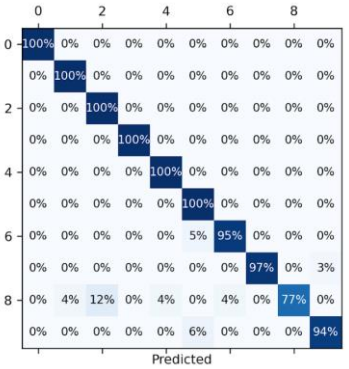

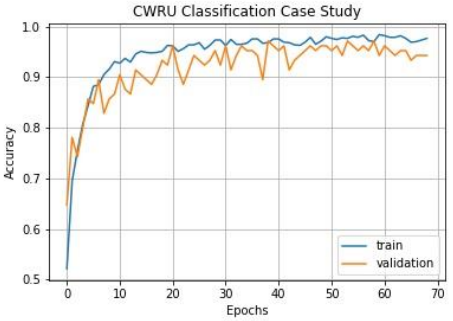

VQE: Ry, Rz, Ry + *i*SWAP (5 layers)

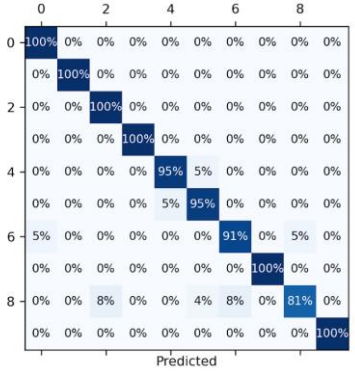

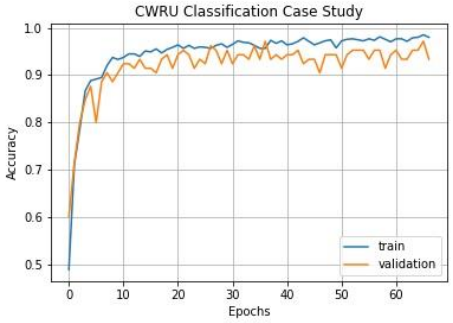

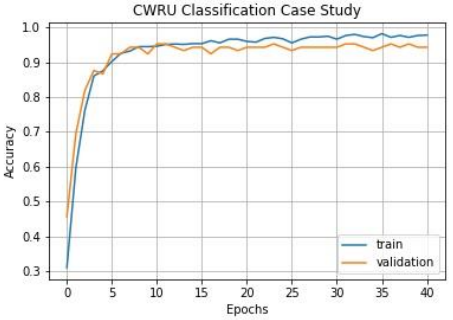

VQE: Ry, Rz, Ry + *i*SWAP (10 layers)